

## **Benthic Cycling of Phosphorus in the Eastern Arabian Sea: Evidence of present day phosphogenesis**

Linsy, P., B. Nagender Nath\*, M.B.L.Mascarenhas-Pereira, Vinitha, P.V., Durbar Ray, C.Prakash Babu, B. Ramalingeswara Rao, Armoury Kazip, Tyson Sebastian, Murlidhar Kocherla, Pavan Miriyala<sup>1</sup>

CSIR – National Institute of Oceanography, Dona Paula, Goa-403 004, India

<sup>1</sup>CSIR – National Geophysical Research Institute, Uppal Road, Hyderabad, India

\*Corresponding author email: [nagender@nio.org](mailto:nagender@nio.org) & [nagendernath@yahoo.com](mailto:nagendernath@yahoo.com)

### **Abstract:**

Results of a study on phosphorus (P) cycling in the Eastern Arabian Sea provides convincing evidence of present-day phosphogenesis in the study area. This finding contrasts with previous reports of the occurrence of only old phosphorites along the Indian margin. Extensive benthic P regeneration is observed in the sediments that are deposited on topographic highs in the western Indian continental margin, which is impinged by a perennial oxygen minimum zone (OMZ). The phosphate flux from the sediments ranged between 1.1 and 22 mmol m<sup>-2</sup> yr<sup>-1</sup>. Among the P reservoirs, biogenic P (P<sub>bio</sub>) is the major pool of P within the upper 30 cm of sediment. P released from organic matter decomposition and fish debris dissolution mainly controls benthic P regeneration while the role of redox cycling of iron is weak. The change in authigenic P (P<sub>auth</sub>) with depth in the sediment and concomitant decrease in porewater dissolved inorganic phosphate (DIP), solid phase P<sub>bio</sub> and organic P (P<sub>org</sub>) content collectively indicate the transformation of P from labile phases to an authigenic phase. Molar C<sub>org</sub>/P<sub>org</sub> and C<sub>org</sub>/P<sub>reactive</sub> ratios also support the notion of ongoing phosphogenesis in the area. The content of carbonate fluoroapatite (CFA) is elevated especially in one of the three study sites as a result of in-situ precipitation and a contribution from eolian and water column authigenesis. The estimated burial efficiency of P at the sediment-water interface at two locations is only about 2%, which is much less than in the western Arabian Sea also indicating extensive P regeneration.

**Keywords:** Phosphogenesis, Benthic flux, Marginal highs, OMZ

## **Introduction:**

Phosphorus (P) is an essential element for marine primary productivity and also acts as a limiting nutrient over geological time scale (Holland, 1978; Broecker and Peng, 1982; Howarth et al., 1995; Tyrrell, 1999). The major sources of P in the ocean are river input, atmospheric deposition and hydrothermal input (e.g., Paytan and Mclaughlin, 2007), while the ultimate sink of P in the ocean is burial within the sediment (Ruttenberg and Berner, 1993). When the buried sediments undergo diagenesis, P is released to the interstitial water and participates in various biogeochemical processes. It may either be recycled back to the water column or get adsorbed on to the surface of metal oxyhydroxides or may precipitate as carbonate fluoroapatite (CFA) which can modulate the benthic flux (e.g., Babu and Nath, 2005).

The Arabian Sea is a highly productive ocean owing to the intense upwelling caused by the southwest monsoon (Qasim, 1982). The high production of organic matter leads to an intense oxygen minimum zone (OMZ) at 150-1200 m water depth in the Arabian Sea (Wyrski, 1973, DeSousa et al., 1996). In addition, the high phytoplankton and zooplankton productivity leads to high fish production in this area (Schenau and De Lange, 2000). All these characteristics make the Arabian Sea a suitable site for studying the pathways of P accumulation in sediments.

The variation in total P in the Arabian Sea sediments has been extensively studied (Murty et al., 1968; Setty and Rao, 1972 and Rao et al., 1978, 1987). Detailed studies of P fractionation and cycling in the area were undertaken in the Eastern Arabian Sea (Babu and Nath, 2005; Acharya et al., 2016), northern part of the Eastern Arabian Sea and the Oman Margin (Schenau et al., 2000; Schenau and De Lange, 2001), and the Western Arabian Sea (Kraal et al., 2012, 2015). The results have shown that the high benthic flux of phosphate in the OMZ is associated with the dissolution of fish debris and degradation of organic matter and may lead to sink switching of P to authigenic phases (Schenau and De Lange, 2001, Babu and Nath, 2005). In addition to organic matter, iron also was found to play a major role in the P cycling and authigenesis in the Arabian Sea sediments (Kraal et al., 2012). A high rate of francolite formation (using porewater fluoride and phosphate gradients and molar P/F ratios in the authigenic fraction) was observed by Schenau et al. (2000) in Oman

Margin sediments leading to the formation of a Holocene phosphorite deposit which contrasted with earlier reports of the occurrence of only old phosphorites in this area (e.g., Rao and Lamboy, 1995).

Rao et al. (1995) and Rao and Rao (1996) reported the occurrence of phosphatic concretions in the marginal high area off Goa (see **Fig.1** for the reported occurrences of phosphorites, phosphogenesis and sediments with high authigenic P). Rao et al. (1995) suggested that the phosphorite in this area is from fish coprolite which was phosphatized under low terrigenous sedimentation rate and calm environmental conditions. They interpreted the phosphorite to be of Pleistocene age and ruled out the possibility of recent formation. Rao and Rao (1996) recovered phosphatic concretions and grains from a sediment core on the same topographic high at different depths but the top 1m sediments did not contain any concretions. The concretions from this core were dated using the U/Th equilibrium method and their ages were estimated to be over 250 ky, no modern concretions were recovered. Nair (1985) has reported the occurrence of Holocene nodular algal limestones containing francolite in other areas of the Eastern Arabian Sea, which he attributed to have been formed from diagenetic processes with the enrichment of phosphate in limestones by microorganisms that built the algal mats. These algal carbonate nodules (**Fig. 1**) with ~ 1 mm thick phosphorite coatings were dated by Borole et al. (1987) using the  $^{230}\text{Th}/^{234}\text{U}$  method and were found to have ages of 5.8-13.9 ky and interpreted to indicate that phosphorite deposition started soon after the carbonate nodule formation. Rao and Lamboy (1996) have, however argued that the phosphatization of these limestones from the eastern Arabian Sea has occurred during a short event in the Early Holocene (at about 8300 yr B.P) influenced by microbial processes following an event of increased terrigenous sediment flux. In a recent study of P speciation in Eastern Arabian Sea sediments, Acharya et al. (2016) have argued for the absence of active phosphatization due to the low total P content and the dominance of a detrital non-reactive fraction of P which would inhibit the formation of authigenic P. This study attempts to assess the P burial pathways and investigate if any phosphogenesis is ongoing in the oxygen depleted sediments of the Eastern Arabian Sea. Three sediment cores raised on three topographic highs from the western continental margin of India. (on one of which the old phosphatic concretions were recovered before by Rao et al. 1995 and Rao and Rao, 1996) are studied here. As they are from topographic highs, they are free from slumping and turbiditic sedimentation.

## Materials and methods

### **Sampling and porewater extraction**

Three short sediment cores were collected from the topographic highs on the Indian continental margin in the central part of the Eastern Arabian Sea during the 40<sup>th</sup> cruise of RV Sindhu Sankalp using a spade corer of 30 x 15 x 50 cm dimensions. (**Fig.2, Table 1**). The cores labeled as SPC 1R, SPC 2 and SPC 4R were recovered from water depths of 347, 325, 279 meters, respectively, within the intense oxygen minimum zone of Arabian Sea (200-1200 m; Wyrтки, 1973).

Undisturbed cores, two from each sampling site, were collected by pushing Plexiglas (6 cm diameter, 40 cm length) into the collected core sediment. The sub-cores were purged with nitrogen and immediately transferred to an onboard chemistry laboratory for the extraction of porewater. The sediments were extruded into a N<sub>2</sub> purged glove-box, sub-sectioned at 2 cm interval, transferred to centrifuge tubes and capped in inert atmosphere. These samples were then centrifuged at 6000 rpm in a refrigerated centrifuge to extract the porewater. The temperature of the centrifuge was set to the in-situ bottom water temperature obtained using CTD data. The porewater was then collected in pre-cleaned vials after filtering through MILLEX HA 0.45 μm pore size cellulose acetate syringe filters in inert conditions and stored in the deep freezer (at -20°C) until the analysis were carried out (which was within few hours after extraction). In addition, sediment sub-cores for geochemical analyses were stored under refrigerated conditions until they were sub-sectioned on the shore laboratory.

Seawater samples were collected from pre-determined depths using a CTD (SBE 25, Seabird, USA) Rosette Sampler fitted with 10 L Niskin bottles. The temperature and salinity of the water column were measured using CTD profiler. Water samples from Niskin bottles were collected for dissolved nutrient and dissolved oxygen (DO) measurements. The samples for DO measurement were fixed immediately using Winkler A and B solution.

### **Chemical analysis of seawater and porewater**

The dissolved oxygen concentration in the seawater samples was measured onboard using Winkler titration method immediately after their collection. DIP in the seawater and porewater were measured using standard spectrophotometric method (Grasshoff et al., 1983). Nitrate concentration in porewater was measured using SKALAR Segmented Flow Auto Analyzer at CSIR-National Institute of Oceanography, India (for method see Parsons et al., 1984). The precision of these analyses is ensured by measuring replicates and triplicates and was within ±3%.

### **Benthic flux and burial efficiency calculation**

Diffusive flux of phosphate at sediment-water interface was calculated by Fick's law of diffusion using the equation

$$J_p = \phi D_s (dC/dZ)$$

where  $J_p$  is the benthic flux of phosphate,  $\phi$  is the porosity calculated from the moisture content data,  $D_s$  is the molecular diffusion coefficient in the sediment and  $dC/dZ$  is the concentration gradient at the sediment water interface.

$$D_s = D^*/\theta^2$$

where  $D^*$  is the diffusion coefficient of  $\text{HPO}_4^{2-}$  in seawater calculated at in situ bottom water temperature (Li and Gregory, 1974), and  $\theta$  is the tortuosity calculated using the equation

$$\theta^2 = 1 - \ln \phi^2 \text{ (Boudreau, 1997).}$$

Phosphorus burial efficiency (PBE) in sediments is calculated using the equation

$$\text{PBE} = 100 \times \text{PAR} / (\text{PAR} + J_p) \text{ (Fang et al., 2007)}$$

where PAR is the phosphorus mass accumulation rate and  $J_p$  is the benthic flux of phosphate.

### **Solid phase analysis**

The core samples were sub-sampled at 1 cm interval and freeze dried. The sediment texture was determined using Laser particle size analyzer after sieving through the 63  $\mu\text{m}$  sieve and treating with acetic acid and hydrogen peroxide to remove carbonates and organic matter respectively. Porosity and dry bulk density were calculated using the moisture content data assuming a particle density of 2.65  $\text{g}/\text{cm}^3$ . Total inorganic carbon (TIC) in the sediments was determined using the  $\text{CO}_2$  coulometer. Total carbon (TC) and total nitrogen in the samples was measured with an elemental analyzer (Thermo Scientific Flash 2000). Total organic carbon (TOC) was calculated by subtracting TIC from TC values. The accuracy of the analysis was determined using a NC reference soil sample. Both the accuracy and precision were within  $\pm 2\%$ .

Trace metal contents in sediments was measured using an Inductively Coupled Plasma Mass Spectrometer (Thermo Fischer ICPMS, X Series 2, Germany) at CSIR- National Institute of Oceanography after digesting it with 7:3:1 HF:  $\text{HNO}_3$ :  $\text{HClO}_4$  acid mixture (MERCK - Suprapur

grade HF and HNO<sub>3</sub>). Total iron content was determined using the Solar S4 Atomic Absorption Spectrophotometer. The accuracy (95%) of the measurements was monitored by analyzing Marine Mud (MAG-1) standard of United States Geological Survey. The texture, trace metals, total iron, TIC and TOC data of SPC 1R and SPC 2 are reported in Chakraborty et al. (2016). Two sections each (one from 3-4 cm and the second one from bottom of the core) were dated using AMS <sup>14</sup>C dating of planktic foraminifera *G. Menardii* at NSF-Arizona AMS Laboratory, USA. For this analysis, the bulk sediments were sieved through 63 micron sieve using ultrapure water and the fraction coarser than 63μ was dried. From this fraction, foraminiferal tests were handpicked under the microscope and sent for dating. The <sup>14</sup>C dates were calibrated to calendar ages using CALPAL 2007.

The detailed P speciation of sediments was carried out using the modified SEDEX procedure by Babu and Nath (2005) (added the step of 2M NH<sub>4</sub>Cl of Schenau and De Lange, (2000) to extract biogenic fish debris to the modified SEDEX method of Anderson and Delaney (2000) which was initially proposed by Ruttenger (1992)). The five sedimentary P pools separated by this technique are (1) P<sub>bio</sub> representing exchangeable or loosely sorbed P and P associated with carbonate and fish debris (2) P<sub>Fe</sub> to represent easily reducible or reactive iron-bound P, (3) P<sub>auth</sub> representing P in authigenic fraction, (4) P<sub>det</sub> representing detrital apatite from break down of rocks of igneous or metamorphic origin and (5) P<sub>org</sub> associated with organic matter. The reactive P (P<sub>react</sub>) was calculated by adding all the fractions except detrital P ( $P_{react} = P_{bio} + P_{Fe} + P_{auth} + P_{org}$ ).

## Results

### Porewater and seawater phosphate

The DIP profiles of the porewater and seawater samples are shown in **Fig. 3**. The porewater DIP profiles of SPC 1R and SPC 2 show similar trends with high concentration in the top 6 cm and low concentration down the core. The porewater DIP concentration in SPC 1R varies between 2-23 μmol/L, whereas in SPC 2 it is between 7-35 μmol/L. In both profiles, highest concentration is observed in the 4-6 cm section. While SPC 1R shows a gradual decrease in DIP concentration after 6 cm, the decrease is more rapid in SPC 2 and becomes almost constant by 10 cm. In SPC 4R, the maximum DIP concentration is observed in the surface (0-2 cm section) and shows a downcore decrease. The concentrations are also low (0.2-7 μmol/L) in this core.

For seawater, the DIP concentration were measured in CTD 1, CTD 2 and CTD 3 corresponding to locations of sediment cores SPC 1R, SPC 2 and SPC 4R respectively. The DIP concentrations at surface are low (**Fig. 3**), with a gradual increase with depth. The values range

between 0.6-5.3, 0.03-2.5 and 0.1-2.8  $\mu\text{mol/L}$  in CTD 1, CTD 2 and CTD 3 respectively. The bottom water DIP values are much lower than those in the porewater of all locations (**Fig. 3**).

### **Benthic flux of phosphate**

The magnitude of benthic flux that are calculated from Fick's law of diffusion for SPC 1R, 2 and 4R are in the order of 16, 22 and 1.1  $\text{mmol m}^{-2}\text{yr}^{-1}$  respectively. Compared to the other two cores SPC 4R has a low benthic flux. However, in all the three locations, the fluxes display negative values, indicating that the flux of phosphate is from the sediment to the water column (**Table 1**).

### **Downcore solid-phase phosphorus profiles**

Downcore variations of sequentially extracted phosphorus fractions and total P contents in three cores are shown in **Fig. 4**.

The total P content in the study area ranges between 42-95  $\mu\text{mol/g}$ . Compared to SPC 1R and SPC 2, total P contents are relatively high in SPC 4R and range from 71-95  $\mu\text{mol/g}$ .

The biogenic P ( $P_{\text{bio}}$ ) content in sediment cores SPC 1R and 2 accounts for 25-50% of total P (**Fig.5**) and varies between 14-28 and 17-43  $\mu\text{mol/g}$  respectively. In SPC 1R,  $P_{\text{bio}}$  fraction shows broad increase at three subsurface depths (at 3-4, 5-7 and 11-13 cm below sea floor (bsf)). In SPC 2,  $P_{\text{bio}}$  content is highest at 5.5 cm bsf (43.3  $\mu\text{mol/g}$ ) and then decreases down the core gradually. In SPC 4R,  $P_{\text{bio}}$  accounts for 20-27% of the total P with values ranging between 15-25  $\mu\text{mol/g}$ . The  $P_{\text{bio}}$  fraction is nearly constant throughout the core with an exception at 13.5 cm bsf, where an increase to 25  $\mu\text{mol/g}$  is observed.

The Fe-bound P ( $P_{\text{Fe}}$ ) in SPC 1R accounts for 9-29 % of total P and varies between 4-16  $\mu\text{mol/g}$ . The  $P_{\text{Fe}}$  content is approximately 9  $\mu\text{mol/g}$  in the top 4 cm with a spike at 5.5 cm (14  $\mu\text{mol/g}$ ) followed by a gradual decrease with depth down to 11 cm with a broad maximum between 11 to 15 cm. The minimum values (4.2 to 6.5  $\mu\text{mol/g}$ ) are found between 16.5 and 22.5 cm with a third increase close to the bottom of the core. In SPC 2,  $P_{\text{Fe}}$  content ranges from 11-27  $\mu\text{mol/g}$  (16-37% of the total P) with a general trend of downcore increase. In SPC 4R, the values ranged between 9-17  $\mu\text{mol/g}$  accounting for 12-22% of the total P.

The authigenic P ( $P_{\text{auth}}$ ) ranges from 2-49  $\mu\text{mol/g}$ . In SPC 1R, the  $P_{\text{auth}}$  content shows great variation from 2-33  $\mu\text{mol/g}$ . The  $P_{\text{auth}}$  content accounts for 3-7% of the total P at the core top but increases up to 51% in the bottom of the core. In SPC 2, the value ranges from 5-28  $\mu\text{mol/g}$  with an

increasing trend down core.  $P_{\text{auth}}$  fraction is very high in SPC 4R and it contributes 36-53% of the total P with values ranging between 28-49  $\mu\text{mol/g}$ .

The detrital ( $P_{\text{det}}$ ) content in the three cores range between 1 and 12  $\mu\text{mol/g}$  and account for not more than 14% of total P. In SPC 1R, the  $P_{\text{det}}$  content is high near the surface and decreases until 8 cm bsf and is then nearly similar for the rest of the core except for a peak at 25 cm bsf. In SPC 2, the values range from 2.6-7.7  $\mu\text{mol/g}$ , accounting for 3-11% of total P. When compared to other two cores, SPC 4R shows higher  $P_{\text{det}}$  content with values ranging between 3.5-12  $\mu\text{mol/g}$ .

The organic P ( $P_{\text{org}}$ ) content ranges from 4-27  $\mu\text{mol/g}$ . In SPC 1R, it is a major contributor to the total P (5-38%) in the surface along with  $P_{\text{bio}}$ .  $P_{\text{org}}$  decreases downcore with values reducing from 27 to 3.6  $\mu\text{mol/g}$  with depth. In SPC 2, the values vary between 4 and 18  $\mu\text{mol/g}$ . In SPC 4R, the variation is less pronounced with values ranging between 3.6 and 6.1  $\mu\text{mol/g}$ .

### **Total iron**

In SPC 1R, the total iron content in carbonate-free basis decreases with depth until 5 cm and then remains nearly constant till 21.5 cm before showing a bottom enrichment (**Fig. 6**) The values range between 3 and 4.8 wt.%. A similar bottom enrichment is seen in core SPC 2 also with values ranging between 3.2 and 7.2 wt.%. In SPC 4R, the values lie in between 4.6 and 7.2 wt.%.

### **Organic and inorganic carbon**

The down core variation of total organic and inorganic carbon (TOC and TIC) are presented in **Fig.7**. The TOC content varies between 2.1 and 10.2 wt.%, 1.3 and 8.8 wt.% and 1.7 and 2.6 wt.% in SPC 1R, 2 and 4R respectively. The TOC profiles of SPC 1R and 2 are similar and illustrate a downward decrease from surface. In contrast, the TOC content in SPC 4R is relatively low and shows no downcore change. The TIC profiles of these three cores mirror image the TOC profiles with values varying between 3.93-9.36 wt.%, 4.7-8.6 wt.% and 9-10 wt.% in SPC 1R, 2 and 4R respectively.



## Discussion

### Benthic flux and solid phase P speciation

The benthic porewater flux values are similar to the previously reported values from the Arabian Sea and the Peruvian OMZ (Schenau and De Lange, 2001; Noffke et al., 2012). Benthic fluxes of phosphate in OMZ sediments are high compared to the sediments below the OMZ, indicating the rapid regeneration of phosphorus in sediments impinged by oxygen depleted waters (Schenau and De Lange, 2001). Compared to SPC 1R and SPC 2, the phosphate flux is less at the location of SPC 4R (**Table 1**), which may be due to the low organic matter and fish debris content ( $P_{\text{bio}}$ ). The high porewater phosphate concentration (**Fig. 3**) in the top layers of the cores may either be due to the increased remineralization of phosphate from organic matter or the release of phosphate from the dissolution of biogenic apatite. The downcore decrease in porewater P concentration is likely the result of the formation of calcium fluorapatite (Jahnke et al., 1983; Ruttenger and Berner, 1993; Schenau et al., 2000).

Our solid phase fractionation results indicate that  $P_{\text{bio}}$  is the major fraction of sedimentary P in the top sections of SPC 1R and 2 while  $P_{\text{auth}}$  is the dominant phase in the bottom depths. SPC 4R is an exception to this pattern with  $P_{\text{auth}}$  as the major fraction throughout the core (**Fig. 5**). Incidentally, the sediment characteristics of this core (SPC 4R) which was recovered from a marginal high off Mangalore region (south of SPC 1R and 2 - **Fig. 2**) differ in the texture (more coarser), sedimentation rate (faster) and TIC content (higher) compared to SPC 1R and 2. The possible reasons are explained in the later part of the paper.

The Arabian Sea is characterized by intense coastal upwelling and high productivity. High amounts of fish debris are found in sediments of upwelling areas (De Vries and Percy, 1982), which is likely the reason for higher  $P_{\text{bio}}$  contents. The decrease in  $P_{\text{bio}}$  content with depth indicates dissolution of biogenic apatite. Even though dissolution of fish debris is proposed to explain the downcore decrease in  $P_{\text{bio}}$ , no DIP increase is seen in the porewater profiles, implying that phosphate released from fish debris is leading to precipitation of authigenic apatite (e.g., Suess, 1981, Schenau et al., 2000) as reflected in the downcore increase in  $P_{\text{auth}}$  content in SPC 1R and SPC 2. Though  $P_{\text{org}}$  forms the third largest P pool in these sediments, a distinct downcore decrease (**Fig. 5**) suggests a major role of this phase in P diagenesis (please see Filippelli et al., 1994; Ingall and Jahnke, 1994; Filippelli and Delaney, 1995, 1996; Filippelli, 2001). The downcore decrease in TOC and  $P_{\text{org}}$  in the cores indicates the degradation and release of P to the porewater, which would enhance the benthic flux of P and would facilitate the formation of authigenic apatite (Froelich et al., 1988; Filippelli et

al., 1994; Ingall and Jahnke, 1994; Filippelli and Delaney, 1995,1996; Filippelli, 2001; Arning et al., 2009a, 2009b). Molar  $C_{org}/P_{org}$  ratios in general are greater than the Redfield ratio (C:P= 106:1) in all the three cores indicating the preferential release of P relative to carbon during organic matter degradation (Schenau and De Lange, 2001; Babu and Nath, 2005). To account for P bound to other reactive forms (such as biogenic, iron bound and authigenic),  $C_{org}/P_{reactive}$  has also been used (Anderson et al., 2001). The molar  $C_{org}/P_{reactive}$  ratio in SPC 1R and SPC 2 is close to the Redfield ratio at surface and decreases down the core (**Fig. 8**), indicating that the transformation of phosphorus is taking place from labile to authigenic phase. Such a sink switching phenomenon from labile to authigenic P phase has been reported before (Ruttenberg and Berner, 1993; Slomp et al., 1996; Louchouart et al., 1997; Babu and Nath, 2005). Much lower  $C_{org}/P_{reactive}$  ratios in SPC 4R (**Fig. 8**) are driven by high  $P_{auth}$  content (**Fig. 4**).

Iron oxyhydroxides play a major role in the benthic cycling of phosphorus. The presence of Fe-oxyhydroxides in the sediment acts as an effective trap of reactive phosphorus. In oxic environments, Fe-oxyhydroxides scavenge the dissolved phosphorus from seawater and porewater. Under reducing conditions, it undergoes reductive dissolution and releases phosphorus to porewater and thereby enhancing the benthic P flux and fueling  $P_{auth}$  formation (Slomp et al., 1996; Filippelli, 2001). But in this study, even under the reducing conditions as deduced from the bottom water oxygen concentration, the  $P_{Fe}$  content does not show a prominent downcore decrease but accounts for 9-37% of the total P (**Fig. 4**). The possible reason for the high  $P_{Fe}$  content at subsurface depths may be the formation of vivianite since the  $P_{Fe}$  fraction can contain Fe-P mineral phases (such as vivianite) along with P associated with iron-oxyhydroxides. It is pertinent to mention here the recent finding of Kraal et al. (2017) that the P extracted during the step targeting Fe-bound P can also extract  $CaCO_3$ -associated P. The formation of vivianite is likely to occur in non sulfidic environments such as below the sulphate methane transition zone (März et al., 2008; Slomp et al., 2013). Dissolved oxygen in the present day Arabian Sea is almost completely consumed, which is accompanied by significant denitrification in the OMZ (150-1200m) (e.g., Naqvi et al., 1993), with no sulfate reduction taking place in the outer shelf (hypoxia) and over the mid shelf (suboxia) (Naqvi, 2008). Also, no euxinic conditions were found to develop in the OMZ in the Arabian Sea during the last 120 kyr (Schenau et al., 2002). The permanent oxygen minimum zone and non-sulfidic condition of the Arabian Sea allows the availability of dissolved Fe for the formation of vivianite. Vivianite would be in the range of 0.11 to 0.66% even if all the  $P_{Fe}$  is converted to vivianite. We have no direct evidence of vivianite because it is below the detection capacity of X-ray diffractometry (~5%). The possibility of Fe oxidation during sample handling may lead to a possible

increase in  $P_{Fe}$  fraction (Kraal et al., 2009; Dijkstra et al., 2014; Kraal and Slomp, 2014). The prevalence of non-sulfidic conditions in the study area preclude Fe sulfide formation ruling out the possibility of oxidation effects on P speciation.

In sediments, the ratio of Fe to P can reflect the changing redox conditions (Louchouart et al., 1997). Schenau and De Lange (2001) use the molar ratio of  $Fe_{CDB}/P_{Fe}$  as a proxy for the reductive dissolution of iron oxyhydroxides. In the absence of  $Fe_{CDB}$  data, we use the  $Fe_{ex}/P_{Fe}$  ratio, in which  $Fe_{ex}$  represents the proportion of Fe in excess of what can be contributed by the residual phase (calculated using Fe and Ti to account for Fe which is non-lithogenic; Murray and Leinen, 1993). The  $Fe_{ex}/P_{Fe}$  shows low values in SPC 2 (7.7-34.8, average-20.6) and SPC 4R (8.9-50.9, average-27.6) (**Fig. 9**). The top 5 cm of sediment at stations SPC 1R stands out in two ways: (1) a down-core decrease in  $Fe_{ex}/P_{Fe}$  from about 46 to 10 (**Fig. 9**) and (2) corresponding increase in porewater DIP (**Fig. 3**) suggesting that a reductive dissolution of iron bound P releases phosphate to the porewater. This interpretation is consistent with the redox conditions within the core. Water column DO values and moderately high porewater nitrate (secondary terminal electron acceptor for organic matter decomposition) plus nitrite values in surface sediments indicate suboxic conditions (**Fig. 9**). The drastic decrease in porewater nitrate plus nitrite values below the surface indicate the near complete utilization of oxygen for the mineralization of organic matter. This is also supported by the increasing U/Th ratio down core from suboxic at surface to anoxic at about 5cm bsf (**Fig. 9**). The ratio of U to Th is commonly used as a redox indicator (Wright et al., 1984; Jones and Manning, 1994 and references therein, Nath et al., 1997; Pattan et al., 2017 and references therein). Since Th is immobile in low-temperature environments, the ratio is sensitive to changes in U supplied from seawater. In turn, U variation depends on the redox state of seawater, with fixation of low valency U under reducing conditions. U/Th ratios above 1.25 have been used to infer suboxic and anoxic conditions and those below 0.75 are indicative of oxic conditions (Jones and Manning, 1994). High porewater nitrate, lower U/Th ratio and higher  $Fe_{ex}/P_{Fe}$  in the core top of SPC 1R collectively indicate that P is probably bound to Fe-oxides/oxyhydroxides in the surface sediments (**Fig. 9**). Such high  $Fe_{ex}/P_{Fe}$  is not found at the other two locations. A gradual reduction in  $P_{Fe}$  content from 5 to 10 cm at SPC 1R is followed by a small increase in  $P_{auth}$  (**Fig. 4**) at about 10 cm indicating that  $P_{Fe}$  dissolution is contributing to the formation of a small amount of authigenic apatite. Two subsurface  $P_{Fe}$  peaks are observed, a distinct high occurs at 11-15 cm and the second close to the bottom of the core (**Fig. 4**). Though, Fe redox cycling seems to have a role here, Fe bound P seems to play limited role in P diagenesis compared to that of P bound to organic carbon and biogenic fractions. The documented scenario at the lower boundary of OMZ in the western Arabian Sea (Kraal et al., 2012)

is different to the proposed processes (interpreted from reactive transport modeling), where Fe redox cycling was postulated to play an important role in P retention and subsequent authigenesis (Kraal et al., 2012).

The  $P_{det}$  constitutes only a minor fraction of TP in the study area. The  $P_{det}$  fraction undergoes burial into the sediment without undergoing any alterations and may indicate the changes in depositional conditions. Major detrital P input on these topographic high areas would be through the settling of suspended materials and atmospheric input. In SPC 1R,  $P_{det}$  is high in top 5cm and nearly uniform until the bottom of the core except for a peak at ~25 cm bsf (**Fig. 4**) which coincides with increased Fe content (**Fig. 6**) possibly representing an episode of increased dust deposition. Similarly, two subsurface peaks in SPC 2 and a large fluctuation in SPC 4R likely represent periods of increased atmospheric input. One subsurface  $P_{det}$  peak in SPC 2 co-occurs with a high  $P_{auth}$  (**Fig. 4**). One possible reason could be an increased nutrient input associated with detrital input. Recently, the SEDEX extraction method was found to extract a part of  $P_{auth}$  as  $P_{det}$  leading to under estimation of  $P_{auth}$  (Kraal et al., 2015). This may not be the case here, as the downcore  $P_{det}$  variation (**Fig. 4**) in this study mimics the variability of refractory elements such as Ti, Th and Zr (**Fig. 10**), with the co-occurring peaks representing periods of increased detrital input.

The phosphorus burial efficiency (PBE) was calculated to evaluate the relative roles of regeneration and burial of P in this part of the Arabian Sea. PBE is very low (2.1 and 2.6%) in SPC 1R and SPC 2 compared to that in SPC 4R (90%). Lower burial efficiencies correspond to lower sedimentation rates (3.8 cm/ky in SPC 1R and 2.1 cm/ky in SPC 2 compared to 26.5 cm/ky in SPC 4R) and higher porewater phosphate fluxes out of sediments (16 mmol m<sup>-2</sup> yr<sup>-1</sup> in SPC 1R and 22 mmol m<sup>-2</sup> yr<sup>-1</sup> in SPC 2 compared to 1.1 mmol m<sup>-2</sup> yr<sup>-1</sup> in SPC 4R) indicating higher regeneration. These burial efficiencies (in SPC 1R and SPC 2) in the eastern Arabian Sea off central India are much lower than those reported for the Oman and Pakistan margins (27 -74% - Schenau and De Lange, 2001) and Murray Ridge in the northern Arabian Sea (14% - Kraal et al., 2012) indicating significant P regeneration in this part of the Arabian Sea. Lack of significant diagenesis (see the section of SPC 4R) and high sediment accumulation may be the reason for the higher PBE (90%) in the southern station.

### **Evidence of ongoing phosphogenesis**

The concurrent decrease in  $P_{org}$  and  $P_{bio}$  with increase in  $P_{auth}$  suggest that  $P_{auth}$  is forming at the expense of  $P_{org}$  and  $P_{bio}$  (Ruttenberg and Berner, 1993) and is a direct indication of phosphogenesis occurring in this area. To quantify the  $P_{auth}$  formation from  $P_{org}$  and  $P_{bio}$  depletion,

best fit curves were drawn and the area under the curves was calculated by integration (**Fig. 11**). The best fit curve was made through the logarithmic fit of the form  $y=m_0+m_1*\ln(x)$  where "ln" is the natural (base e) logarithm function (**Fig. 11**). The Trapezoidal numerical integration method was used to calculate the area under the graph. This method approximates the integration over an interval by breaking the area down into trapezoids with more easily computable areas. The depth integrated  $P_{\text{auth}}$  formation and deficit of  $P_{\text{org}}$  and  $P_{\text{bio}}$  were calculated from these values (similar to the approach followed in Ruttenberg and Berner, 1993). The equation for conversion from the area to integrated P gain/deficit and  $R^2$  values for the best fit are given in the **Table 2**. From the data, it is clear that the  $P_{\text{auth}}$  formation (SPC 1R - 0.99, SPC 2-1.09  $\text{gP}/\text{cm}^2$ ) is higher than the  $P_{\text{org}}$  deficit in both SPC 1R and SPC 2 (SPC 1R-0.82, SPC 2-0.51  $\text{gP}/\text{cm}^2$ ) indicating that organic matter degradation is not the only process responsible for the authigenic apatite formation but the biogenic P dissolution also acts as a major contributor. In both sites, however, the sum of  $P_{\text{org}}$  and  $P_{\text{bio}}$  deficit (SPC 1R-2.36, SPC 2-2.19  $\text{gP}/\text{cm}^2$ ) exceeds the integrated  $P_{\text{auth}}$  values, suggesting that the excess release of P from organic matter degradation and fish debris dissolution is responsible for the high benthic fluxes in these locations and  $P_{\text{Fe}}$  exerts only a minor role in authigenesis and benthic fluxes here. In SPC 4R, however, curve fitting was not possible and a downcore profile of  $P_{\text{react}}$  (sum of  $P_{\text{bio}}$ ,  $P_{\text{Fe}}$  and  $P_{\text{org}}$ ) and  $P_{\text{auth}}$  is drawn (**Fig. 12**). Both the profiles follow a similar trend indicating the lack of significant diagenetic transformation of  $P_{\text{react}}$  to  $P_{\text{auth}}$  phase. The depletion of other reactive fractions ( $P_{\text{bio}}$ ,  $P_{\text{Fe}}$  and  $P_{\text{org}}$ ) is not large enough to account for the high  $P_{\text{auth}}$  content of SPC 4R and may involve an external source such as atmospheric deposition.

#### **Atmospheric deposition and controls on P geochemistry in SPC-4R**

In addition to contribution from fish debris and organic matter, atmospheric deposition can contribute Ca-P minerals to the  $P_{\text{auth}}$  pool (Eijsink et al., 2000; Faul et al., 2005; Palastanga et al., 2011; Kraal et al., 2012; März et al., 2014; Ni et al., 2015). Kraal et al., (2012) have in fact reported an important role of atmospheric dust in P deposition in the western Arabian Sea. Atmospheric input of  $P_{\text{auth}}$  is likely in our sediment cores deposited on topographic highs. In core SPC 4R the depositional pattern is different than the other two northern cores as revealed by downcore elemental variation (**Fig. 10**). While the downcore variation of refractory elements (Ti, Th, Zr, Rb) is low and show a near uniform pattern in cores SPC 1R and SPC 2, the concentrations of these elements are high and shows distinct downcore peaks in SPC 4R, documenting periods/episodes of change in lithogenic sedimentation. Incidentally, downcore variation of some P phases including that of  $P_{\text{det}}$  and  $P_{\text{auth}}$  (with a slight offset) also follows the trend of refractory elements corroborating that the P deposition is dominantly driven by depositional change. The episodic changes in depositional

conditions can either be due to lateral advection of lithogenic material from land or due to the eolian input. Lateral advection is unlikely, however, as the distance from shore is about 200 km, and therefore atmospheric deposition may be driving the changes in elemental content. The high Ti and Zr content which are good proxies for dust deposition (see Nath, 2001 and references therein), at SPC 4R may be a result of high atmospheric deposition in this area. The clay mineral palygorskite that is typical of atmospheric deposition was reported to be present in a broad band of sediments extending from Arabia to the southern tip of India (Kolla et al., 1976). A good correlation of peaks in palygorskite content with topographic highs was noticed, and attributed to reflect eolian processes. The trajectories of dust-bearing winds reconstructed for the Holocene has shown a plume reaching from the coast of Yemen up to the southern tip of India (Sirocko et al., 1991) in agreement with the studies of Kolla et al., (1976). The plume is influenced by long-distance transport by north-westerly and westerly winds from Arabia and the Persian Gulf (the Shamal) across the Arabian Sea (Sirocko and Sarnthein, 1989). Palygorskite-rich aerosols move at heights well above the low level southwest monsoon trajectories and transport dust throughout the Arabian Sea (Sirocko et al., 1991). Palygorskite derived from Arabia and Somalia was also reported in the southwest coast of India (Chauhan, 1996), little south of our site. The Arabian Sea receives relatively large fluxes of P through atmospheric input (Okin et al., 2011). According to Kraal et al. (2012), 60%~of the background Ca-P concentration may be of atmospheric origin in the western Arabian Sea. Thus, the likely reason for higher  $P_{\text{auth}}$  values throughout core SPC 4R in conjunction with the lack of direct relation between  $P_{\text{auth}}$  and other reactive P phases may be to the result of deposition of atmospheric dust containing  $P_{\text{auth}}$ . A P-speciation study of settling particles reveals a significant fraction of total P (~ 25%, ranging from 3–78%) is carried from the upper ocean to the sediments as authigenic P (Faul et al., 2005) providing evidence that the remineralization of organic P and the exchange with other forms of P may begin in the water column, and continue in the sediments. A considerable transformation from the organic to the inorganic P pool in the water column was also reported (Paytan et al., 2003).

Though the P-speciation data does not show clear evidences of sink-switching within core SPC 4R, down core depletion of porewater P indicates the utilization of P possibly for authigenic P formation. The highest peak of  $P_{\text{auth}}$  content was observed at 12.5 cm bsf where a depletion in  $P_{\text{org}}$  and porewater DIP occurs suggesting in situ precipitation. Thus, in addition to significant atmospheric deposition, authigenic precipitation is likely taking place in the sediment.

The third process considered here for the high  $P_{\text{auth}}$  content in SPC 4R is winnowing. While Shimmield et al. (1990) and Pedersen et al. (1992) have attributed the high phosphorus concentration

in the top sediment layers of Oman Margin to winnowing, Schenau et al. (2000) have ruled out the role of winnowing for the high phosphorus concentrations in the western Arabian Sea sediments. In winnowing, the high specific gravity of phosphatic precipitate ( $2.9 \text{ g/cm}^3$ ) compared to other sediment particles ( $1.5\text{-}2.5 \text{ g/cm}^3$ ), removes the finer and lighter particles, which leads to the concentration of phosphatic precipitates (Follmi, 1996; Schenau et al., 2000). While no visible phosphatic grains/pellets were found in the core, extrapolated sedimentation rates (AMC  $^{14}\text{C}$  dates of forams) of the core tops yield an age of  $\sim 700$  years BP for SPC 4R compared to 45 years and near zero age for cores SPC 1R and SPC 2 respectively suggesting an intense winnowing at SPC 4R. The high carbonate content (75-83 wt.%) and coarse grained texture along with the high  $C_{\text{org}}/N$  ratio in the top section of SPC 4R (see Schenau et al., 2000) compared to the other two cores also support higher winnowing activity in the area (**Fig. 13**). In summary, the combination of eolian input and water column precipitation, early diagenesis within the sediments, and the winnowing in that order seems to be responsible for the high  $P_{\text{auth}}$  content in core SPC 4R.

Schenau et al. (2000) reported present-day phosphogenesis in the northern part of the Eastern Arabian Sea off the Pakistan coast. The here presented study is to our knowledge the first report of the occurrence of phosphogenesis in the western continental margin of India. While we found geochemical evidence of phosphogenesis, phosphatic pellets/crusts/concretions were not recovered in the studied cores. As mentioned in the introduction, all the phosphorites/concretions/phosphatic limestones recovered so far from the Indian continental margin are of older age (Nair, 1985; Borole et al., 1987; Rao et al., 1995; Rao and Rao, 1996; Rao and Lamboy, 1996; Vaz et al., 1996), with Rao et al., (1995) ruling out the possibility of their recent formation from a P speciation study of the sediments from the same latitudes as ours in the Eastern Arabian Sea but from more shallow locations (depth  $\sim 25\text{m}$ ), Acharya et al. (2016) report the absence of active phosphatization in the area and attribute the lack of authigenic P to low total P content and the dominance of detrital non-reactive P. In our opinion, the absence of active phosphatization/phosphogenesis in their study area is due to the unsuitable locations chosen to study the occurrence of phosphogenesis. The sampling sites are located close to the coast in a shallow water depth (25 and 26 m). Such areas receive high terrigenous sediment input and bottom waters are well oxygenated. At such depths, seasonal hypoxia occurs 2-3 months in a year but bottom waters were well oxygenated during the remaining parts of the year (Naqvi et al., 2009). The oxic bottom water promotes the adsorption of P on iron oxyhydroxide and limits the release of phosphate to the porewater and the subsequent authigenesis. The high sedimentation rates and high terrigenous input to the inner shelf regions will lead to the deposition of non-reactive P. In contrast the topographic highs impinged by less oxygenated waters

such as ours may be suitable for phosphogenesis. The Eastern Arabian Sea has several such structural highs (e.g., Mukhopadhyay et al., 2008; Rao et al., 2010), which are potential sites for the occurrence of phosphogenesis and phosphorite formation.

## Conclusions

Porewater phosphate and solid-phase P speciation results indicate that rapid regeneration of phosphorus is occurring in the sediments on topographic highs that are impinged by poorly oxygenated waters in the eastern Arabian Sea. Benthic regeneration of phosphorus is induced by high rate of organic matter degradation and fish debris dissolution. Redox cycling of iron has a limited influence on the sedimentary P cycling in this area. High concentrations of authigenic P (suggesting CFA precipitation) were measured in the sediment. Molar  $C_{\text{org}}/P_{\text{org}}$  and  $C_{\text{org}}/P_{\text{reactive}}$  ratios indicate the transformation from reactive P to authigenic P. In addition to the enhanced degradation of organic material and the dissolution of fish debris, low sedimentation rates and oxygen depleted conditions favor the ongoing phosphogenesis. The here presented finding of present-day phosphogenesis and the earlier reports of occurrence of older phosphorites during different periods of the Pleistocene collectively indicate that the marginal highs overlain by poorly oxygenated waters in the Eastern Arabian Sea could be important sites of P burial, in particular during periods of increased productivity. At one of our study sites, atmospheric input of P and formation of authigenic P in the water column may have contributed to the high concentrations of authigenic P observed in the sediment.

## Acknowledgements

The authors thank all the shipboard participants who helped during the sampling and operations, Director, CSIR-NIO for permission to publish and for providing the ship time, Shri Kartheek Chennuri and Dr. G.Parthiban for ICP-MS analyses and Dr. Rahul Sharma for salary support from GAP-2128 to LP. The comments from Dr. Peter Kraal and an anonymous reviewer have helped in improving the quality of this paper significantly. Thanks are due to Editor-in-Chief Dr. T.Bianchi and the Associate Editor Dr. C.P.Slomp for their positive evaluation. Dr. Gregory Eberli (University of Miami) is thanked for his time in making the manuscript more readable. All the



analytical expenses were met from PSC-0106 to fulfill the objectives of CSIR XII Plan Project GEOSINKS. This is NIO Contribution No. XXXX

## References

- Acharya, S.S., Panigrahi, M.K., Kurian, J., Gupta, A.K., Tripathy, S., 2016. Speciation of phosphorus in the continental shelf sediments in the Eastern Arabian Sea. *Cont. Shelf Res.* 115, 65–75. doi:10.1016/j.csr.2016.01.005
- Anderson, L.D., Delaney, M.L., 2000. Sequential extraction and analysis of phosphorus in marine sediments: Streamlining of the SEDEX procedure. *Limnol. Oceanogr.* 45, 509–515. doi:10.4319/lo.2000.45.2.0509
- Anderson, L.D., Delaney, M.L., Faul, K.L., 2001. Carbon to phosphorus ratios in sediments: Implications for nutrient cycling. *Global Biogeochem. Cycles* 15, 65–79. doi:10.1029/2000GB001270
- Babu, C.P., Nath, B.N., 2005. Processes controlling forms of phosphorus in surficial sediments from the eastern Arabian Sea impinged by varying bottom water oxygenation conditions. *Deep Sea Res. Part II Top. Stud. Oceanogr.* 52, 1965–1980. doi:10.1016/j.dsr2.2005.06.004
- Borole, D., Rajagopalan, G., Somayajulu, B.L., 1987. Radiometric ages of phosphorites from the west coast of India. *Mar. Geol.* 78, 161–165. doi:10.1016/0025-3227(87)90075-2
- Boudreau, B.P., 1997. *Diagenetic models and their implementation*. Springer Berlin.
- Broecker, W.S., Peng, T.H., 1982. *Tracers in the Sea*, Eldigio, Lamont-Doherty Geol. Obs. Columbia Univ., Palisades, NY.
- Chakraborty, P., Vudamala, K., Chennuri, K., Armoury, K., Linsy, P., Ramteke, D., Sebastian, T., Jayachandran, S., Naik, C., Naik, R., Nath, B.N., 2016. Mercury profiles in sediment from the marginal high of Arabian Sea: an indicator of increasing anthropogenic Hg input. *Environ. Sci. Pollut. Res.* 23, 8529–8538. doi:10.1007/s11356-015-5925-1
- Chauhan, O.S., 1996. Aeolian deposition of Arabia and Somalia sediments on the southwestern continental margin of India. *Curr. Sci.* 71, 233–236. doi:10.2307/24099588
- De Vries, T.J., Percy, W.G., 1982. Fish debris in sediments of the upwelling zone off central Peru: a late Quaternary record. *Deep Sea Res. Part A, Oceanogr. Res. Pap.* 29, 87–109. doi:10.1016/0198-0149(82)90063-2
- DeSousa, S.N., DileepKumar, M., Sardessai, S., Sarma, V.V.S.S., Shirodkar, P.V., 1996. Seasonal variability in oxygen and nutrients in the central and eastern Arabian Sea. *Curr. Sci.* 71, 847–851.
- Dijkstra, N., Kraal, P., Kuypers, M.M.M., Schnetger, B., Slomp, C.P., 2014. Are iron-phosphate minerals a sink for phosphorus in anoxic Black Sea sediments? *PLoS One* 9, 1–12.

doi:10.1371/journal.pone.0101139

- | Eijssink, L.M., Krom, M.D., Herut, B., 2000. Speciation and burial flux of phosphorus in the surface sediments of the Eastern Mediterranean. *Am. Journal Sci.* 300, 483–503.
- | Fang, T., Chen, J., Huh, C., 2007. Sedimentary phosphorus species and sedimentation flux in the East China Sea. *Cont. Shelf Res.* 27, 1465–1476. doi:10.1016/j.csr.2007.01.011
- | Faul, K.L., Paytan, A., Delaney, M.L., 2005. Phosphorus distribution in sinking oceanic particulate matter. *Mar. Chem.* 97, 307–333. doi:10.1016/j.marchem.2005.04.002
- | Filippelli, G.M., 2001. Carbon and phosphorus cycling in anoxic sediments of the Saanich Inlet, British Columbia. *Mar. Geol.* 174, 307–321. doi:10.1016/S0025-3227(00)00157-2
- | Filippelli, G.M., Delaney, M.L., 1996. Phosphorus geochemistry of equatorial Pacific sediments. *Geochim. Cosmochim. Acta* 60, 1479–1495. doi:10.1016/0016-7037(96)00042-7
- | Filippelli, G.M., Delaney, M.L., 1995. Phosphorus geochemistry and accumulation rates in the Eastern Equatorial Pacific Ocean: Results from Leg 138. *Proc. Ocean Drill. Program, Sci. Results* 138, 757–767.
- | Filippelli, G.M., Delaney, M.L., Garrison, R.E., Omarzai, S.K., Behl, R.J., 1994. Phosphorus accumulation rates in a Miocene low oxygen basin: The Monterey Formation (Pismo Basin), California. *Mar. Geol.* 116, 419–430. doi:10.1016/0025-3227(94)90055-8
- | Follmi, K., 1996. The phosphorus cycle, phosphogenesis and marine phosphate-rich deposits. *Earth-Science Rev.* 40, 55–124. doi:10.1016/0012-8252(95)00049-6
- | Froelich, P.N., Arthur, M.A., Burnett, W.C., Deakin, M., Hensley, V., Jahnke, R., Kaul, L., Kim, K.H., Roe, K., Soutar, A., Vathakanon, C., 1988. Early diagenesis of organic matter in Peru continental margin sediments: Phosphorite precipitation. *Mar. Geol.* 80, 309–343. doi:10.1016/0025-3227(88)90095-3
- | Grasshoff, K., Ehrhardt, M., Kremling, K., 1983. *Methods of seawater analysis*, 419 pp, Verlag Chemie, New York.
- | Holland, H.D., 1978. *The chemistry of the atmosphere and oceans*. Wiley, New York, NY.
- | Howarth, R.W., Jensen, H.S., Marino, R., Postma, H., 1995. Transport to and processing of P in near-shore and oceanic waters, in: Tiessen, H. (Ed.), *Phosphorus in the Global Environment: Transfers, Cycles, and Management*. John Wiley & Sons, Chichester, England, p. 323–345 (SCOPE; No. 54).
- | Ingall, E., Jahnke, R., 1994. Evidence for enhanced phosphorus regeneration from marine sediments overlain by oxygen depleted waters. *Geochim. Cosmochim. Acta* 58, 2571–2575. doi:10.1016/0016-7037(94)90033-7
- | Jahnke, R.A., Emerson, S.R., Roe, K.K., Burnett, W.C., 1983. The present day formation of apatite in Mexican continental margin sediments. *Geochim. Cosmochim. Acta* 47, 259–266. doi:10.1016/0016-7037(83)90138-2
- | Jones, B., Manning, D.A.C., 1994. Comparison of geochemical indices used for the interpretation of

palaeoredox conditions in ancient mudstones. *Chem. Geol.* 111, 111–129. doi:10.1016/0009-2541(94)90085-X

- | Kolla, V., Henderson, L., Biscaye, P.E., 1976. Clay mineralogy and sedimentation in the western Indian ocean. *Deep Sea Res. Oceanogr. Abstr.* 23, 949–961. doi:10.1016/0011-7471(76)90825-1
- | Kraal, P., Bostick, B.C., Behrends, T., Reichart, G.J., Slomp, C.P., 2015. Characterization of phosphorus species in sediments from the Arabian Sea oxygen minimum zone: Combining sequential extractions and X-ray spectroscopy. *Mar. Chem.* 168, 1–8. doi:10.1016/j.marchem.2014.10.009
- | Kraal, P., Dijkstra, N., Behrends, T., Slomp, C.P., 2017. Phosphorus burial in sediments of the sulfidic deep Black Sea: Key roles for adsorption by calcium carbonate and apatite authigenesis. *Geochim. Cosmochim. Acta* 204, 140–158. doi:10.1016/j.gca.2017.01.042
- | Kraal, P., Slomp, C.P., 2014. Rapid and Extensive Alteration of Phosphorus Speciation during Oxidative Storage of Wet Sediment Samples. *PLoS One* 9, 1–6. doi:10.1371/journal.pone.0096859
- | Kraal, P., Slomp, C.P., Forster, A., Kuypers, M.M.M., Sluijs, A., 2009. Pyrite oxidation during sample storage determines phosphorus fractionation in carbonate-poor anoxic sediments. *Geochim. Cosmochim. Acta* 73, 3277–3290. doi:10.1016/j.gca.2009.02.026
- | Kraal, P., Slomp, C.P., Reed, D.C., Reichart, G.J., Poulton, S.W., 2012. Sedimentary phosphorus and iron cycling in and below the oxygen minimum zone of the northern Arabian Sea. *Biogeosciences* 9, 2603–2624. doi:10.5194/bg-9-2603-2012
- | Li, Y.-H., Sandra Gregory, 1974. Diffusion of ions in sea water and in deep-sea sediments. *Geochim. Cosmochim. Acta* 38, 703–714.
- | Louchouart, P., Lucotte, M., Duchemin, E., De Vernal, A., 1997. Early diagenetic processes in recent sediments of the Gulf of St-Lawrence: Phosphorus, carbon and iron burial rates. *Mar. Geol.* 139, 181–200. doi:10.1016/S0025-3227(96)00110-7
- | März, C., Hoffmann, J., Bleil, U., de Lange, G.J., Kasten, S., 2008. Diagenetic changes of magnetic and geochemical signals by anaerobic methane oxidation in sediments of the Zambesi deep-sea fan (SW Indian Ocean). *Mar. Geol.* 255, 118–130. doi:10.1016/j.margeo.2008.05.013
- | März, C., Poulton, S.W., Wagner, T., Schnetger, B., Brumsack, H.J., 2014. Phosphorus burial and diagenesis in the central Bering Sea (Bowers Ridge, IODP Site U1341): Perspectives on the marine P cycle. *Chem. Geol.* 363, 270–282. doi:10.1016/j.chemgeo.2013.11.004
- | Mukhopadhyay, R., Rajesh, M., De, S., Chakraborty, B., Jauhari, P., 2008. Structural highs on the western continental slope of India: Implications for regional tectonics. *Geomorphology* 96, 48–61. doi:10.1016/j.geomorph.2007.07.017
- | Murray, R.W., Leinen, M., 1993. Chemical transport to the seafloor of the equatorial Pacific Ocean across a latitudinal transect at 135°W: Tracking sedimentary major, trace, and rare earth element fluxes at the Equator and the Intertropical Convergence Zone. *Geochim. Cosmochim. Acta* 57, 4141–4163. doi:10.1016/0016-7037(93)90312-K

- | Murty, P.S.N., Reddy, C.V.G., Varadachari, V.V.R., 1968. Distribution of total phosphorus in the shelf sediments off the west coast of India, in: Proc. Nat. Inst. Sci. India. pp. 134–141.
- | Nair, R.R., 1985. Holocene phosphorites of the western continental margin of India. *Mahasagar* 18, 273–279.
- | Naqvi, S.W.A., 2008. The Indian Ocean, in: Capone, D.G., Bronk, D.A., Mulholland, M.R., Carpenter, E. (Eds.), *Nitrogen in the Marine Environment*. Elsevier, Amsterdam; The Netherlands, pp. 631–681.
- | Naqvi, S.W.A., Kumar, M.D., Narvekar, P. V., De Sousa, S.N., George, M.D., D’Silva, C., 1993. An intermediate nepheloid layer associated with high microbial metabolic rates and denitrification in the northwest Indian Ocean. *J. Geophys. Res.* 98, 16469. doi:10.1029/93JC00973
- | Naqvi, S.W.A., Naik, H., Jayakumar, A., Pratihary, A.K., Narvekar, G., Kurian, S., Agnihotri, R., Shailaja, M.S., Narvekar, P. V., 2009. Seasonal anoxia Over the Western Indian Continental Shelf. *American Geophysical Union*, pp. 333–345. doi:10.1029/2008GM000745
- | Nath, B.N., 2001. Geochemistry of sediments, in: Sen Gupta, R., Desa, E. (Eds.), *The Indian Ocean : A Perspective*. A.A. Balkema, pp. 645–690.
- | Nath, B.N., Bau, M., Ramalingeswara Rao, B., Rao, C.M., 1997. Trace and rare earth elemental variation in Arabian Sea sediments through a transect across the oxygen minimum zone. *Geochim. Cosmochim. Acta* 61, 2375–2388. doi:10.1016/S0016-7037(97)00094-X
- | Ni, J., Lin, P., Zhen, Y., Yao, X., Guo, L., 2015. Distribution, source and chemical speciation of phosphorus in surface sediments of the central Pacific Ocean. *Deep Sea Res. Part I Oceanogr. Res. Pap.* 105, 74–82. doi:http://dx.doi.org/10.1016/j.dsr.2015.08.008
- | Noffke, A., Hensen, C., Sommer, S., Scholz, F., Bohlen, L., Mosch, T., Graco, M., Wallmann, K., 2012. Benthic iron and phosphorus fluxes across the Peruvian oxygen minimum zone. *Limnol. Oceanogr.* 57, 851–867. doi:10.4319/lo.2012.57.3.0851
- | Okin, G.S., Baker, A.R., Tegen, I., Mahowald, N.M., Dentener, F.J., Duce, R.A., Galloway, J.N., Hunter, K., Kanakidou, M., Kubilay, N., Prospero, J.M., Sarin, M., Surapipith, V., Uematsu, M., Zhu, T., 2011. Impacts of atmospheric nutrient deposition on marine productivity: Roles of nitrogen, phosphorus, and iron. *Global Biogeochem. Cycles* 25. doi:10.1029/2010GB003858
- | Palastanga, V., Slomp, C.P., Heinze, C., 2011. Long-term controls on ocean phosphorus and oxygen in a global biogeochemical model. *Global Biogeochem. Cycles* 25, 1–19. doi:10.1029/2010GB003827
- | Parsons, T.R., Malta, Y., Lalli, C.M., 1984. *A Manual of Chemical and Biological Methods for Seawater Analysis*. Pergamon Press New York.
- | Pattan, J.N., Parthiban, G., Garg, A., Moraes, N.R.C., 2017. Intense reducing conditions during the last deglaciation and Heinrich events (H1, H2, H3) in sediments from the oxygen minimum zone off Goa, eastern Arabian Sea. *Mar. Pet. Geol.* 84, 243–256. doi:10.1016/j.marpetgeo.2017.03.034
- | Paytan, A., Cade-menun, B.J., McLaughlin, K., Faul, K.L., 2003. Selective phosphorus regeneration

of sinking marine particles: evidence from 31 P-NMR. *Mar. Chem.* 82, 55–70. doi:10.1016/S0304-4203(03)00052-5

- | Paytan, A., Mclaughlin, K., 2007. The Oceanic Phosphorus Cycle. *Chem. Rev.* 107, 563–576. doi:10.1021/cr0503613
- | Pedersen, T., Shimmield, G., N.B, P., 1992. Lack of enhanced preservation of organic matter in sediments under the oxygen minimum on the Oman Margin. *Geochim. Cosmochim. Acta* 56, 545–551. doi:10.1016/0016-7037(92)90152-9
- | Qasim, S.Z., 1982. Oceanography of the northern Arabian Sea. *Deep Sea Res. Part A, Oceanogr. Res. Pap.* 29, 1041–1068. doi:10.1016/0198-0149(82)90027-9
- | Rao, C.M., Paropkari, A.L., Mascarenhas, A., Murty, P.S.N., 1987. Distribution of phosphorus and phosphatisation along the western continental margin of India. *J. Geol. Soc. India* 30, 423–438.
- | Rao, C.M., Rajamanickam, G. V, Paropkari, A.L., Murty, P.S.N., 1978. Distribution of phosphate in sediments of the northern half of the western continental shelf of India. *Indian J. Mar. Sci.* 7, 146–150.
- | Rao, C.M., Rao, B.R., 1996. Phosphorite concretions in a sediment core from a bathymetric high off Goa, western continental margin of India. *Curr. Sci.* 70, 308–312.
- | Rao, D.G., Paropkari, A.L., Krishna, K.S., Chaubey, A.K., Ajay, K.K., Kodagali, V.N., 2010. Bathymetric highs in the mid-slope region of the western continental margin of India— Structure and mode of origin. *Mar. Geol.* 276, 58–70. doi:10.1016/j.margeo.2010.07.007
- | Rao, V.P., 1986. Phosphorites from the Error Seamount, Northern Arabian Sea. *Mar. Geol.* 71, 177–186. doi:10.1016/0025-3227(86)90038-1
- | Rao, V.P., Hegner, E., Wajih, S., Naqvi, A., Mohan, P., Masood, S., Suryanarayana, D., 2008. Miocene phosphorites from the Murray Ridge, northwestern Arabian Sea. *Palaeogeogr. Palaeoclimatol. Palaeoecol.* 260, 347–358. doi:10.1016/j.palaeo.2007.12.003
- | Rao, V.P., Kessarkar, P.M., Nagendra, R., Babu, E.V.S.S.K., 2007. Origin of Cretaceous phosphorites from the onshore of Tamil Nadu, India. *J. Earth Syst. Sci.* 116, 525–536. doi:10.1007/s12040-007-0048-9
- | Rao, V.P., Lamboy, M., 1995. Phosphorites from the oman margin, ODP Leg-117. *Oceanol. Acta* 18, 289–307.
- | Rao, V.P., Lamboy, M., 1996. Genesis of apatite in the phosphatized limestones of the western continental shelf of India. *Mar. Geol.* 136, 41–53. doi:10.1016/S0025-3227(96)00062-X
- | Rao, V.P., Michard, A., Naqvi, S.W.A., Bottcher, M.E., Krishnaswamy, R., Thamban, M., Natarajan, R., Borole, D. V, 2002. Quaternary phosphorites off the southeast coast of India. *Chem. Geol.* 182, 483–502.
- | Rao, V.P., Nair, R.R., 1988. Microbial origin of the phosphorites of the western continental shelf of India. *Mar. Geol.* 84, 105–110. doi:10.1016/0025-3227(88)90128-4
- | Rao, V.P., Rao, C.M., Thamban, M., Natarajan, R., Rao, B.R., 1995. Origin and significance of high-

grade phosphorite in a sediment core from the continental slope off Goa, India. *Curr. Sci.* 69, 1017–1022.

- | Rao, V.P., Rao, K.M., Raju, D.S.N., 2000. Quaternary Phosphorites from the Continental Margin Off Chennai, Southeast India: Analogs of Ancient Phosphate Stromatolites. *J. Sediment. Res.* 70, 1197–1209. doi:10.1306/012400701197
- | Rao, V.P., Rao, K.M., Vora, K.H., Almeida, F., Subramaniam, M.M., Souza, C.G.A., 1998. A potential phosphorite deposit on the continental margin off Chennai. *Curr. Sci.* 74, 574–577.
- | Ruttenberg, C., 1992. Development of a sequential extraction method for different forms of phosphorus in marine sediments. *Limnol. Oceanogr.* 37, 1460–1482.
- | Ruttenberg, K.C., Berner, R.A., 1993. Authigenic apatite formation and burial in sediments from non-upwelling, continental margin environments. *Geochim. Cosmochim. Acta* 57, 991–1007. doi:10.1016/0016-7037(93)90035-U
- | Schenau, S.J., De Lange, G.J., 2001. Phosphorus regeneration vs . burial in sediments of the Arabian Sea. *Mar. Chem.* 75, 201–217.
- | Schenau, S.J., De Lange, G.J., 2000. A novel chemical method to quantify fish debris in marine sediments. *Limnol. Oceanogr.* 45, 963–971.
- | Schenau, S.J., Passier, H.F., Reichart, G.J., de Lange, G.J., 2002. Sedimentary pyrite formation in the Arabian Sea. *Mar. Geol.* 185, 393–402. doi:10.1016/S0025-3227(02)00183-4
- | Schenau, S.J., Slomp, C.P., Lange, G.J. De, 2000. Phosphogenesis and active phosphorite formation in sediments from the Arabian Sea oxygen minimum zone. *Mar. Geol.* 169, 1–20.
- | Setty, M., Rao, C.M., 1972. Phosphate, carbonate and organic matter distribution in sediment cores off Bombay–Saurashtra coast, India, in: *Twenty-Fourth International Geological Congress*, Canada. pp. 182–191.
- | Shimmield, G.B., Mowbray, S.R., Weedon, G.P., 1990. A 350 ka history of the Indian Southwest Monsoon—evidence from deep-sea cores, northwest Arabian Sea. *Trans. R. Soc. Edinb. Earth Sci.* 81, 289–299. doi:10.1017/S0263593300020800
- | Sirocko, F., Sarnthein, M., 1989. Wind-Borne Deposits in the Northwestern Indian Ocean: Record of Holocene Sediments Versus Modern Satellite Data, in: Leinen, M., Sarnthein, M. (Eds.), *Paleoclimatology and Paleometeorology: Modern and Past Patterns of Global Atmospheric Transport*. Springer Netherlands, Dordrecht, pp. 401–433. doi:10.1007/978-94-009-0995-3\_17
- | Sirocko, F., Sarnthein, M., Lange, H., Erlenkeuser, H., 1991. Atmospheric summer circulation and coastal upwelling in the Arabian Sea during the Holocene and the last glaciation. *Quat. Res.* 36, 72–93. doi:10.1016/0033-5894(91)90018-Z
- | Slomp, C.P., Mort, H.P., Jilbert, T., Reed, D.C., Gustafsson, B.G., Wolthers, M., 2013. Coupled Dynamics of Iron and Phosphorus in Sediments of an Oligotrophic Coastal Basin and the Impact of Anaerobic Oxidation of Methane. *PLoS One* 8. doi:10.1371/journal.pone.0062386
- | Slomp, C.P., Van der Gaast, S.J., Van Raaphorst, W., 1996. Phosphorus binding by poorly crystalline iron oxides in North Sea sediments. *Mar. Chem.* 52, 55–73. doi:10.1016/0304-

4203(95)00078-X

- | Suess, E., 1981. Phosphate regeneration from sediments of the Peru continental margin by dissolution of fish debris. *Geochim. Cosmochim. Acta* 45, 577–588. doi:10.1016/0016-7037(81)90191-5
- | Tyrrell, T., 1999. The relative influences of nitrogen and phosphorus on oceanic primary production. *Nature* 400, 525–531. doi:10.1038/22941
- | Vaz, G.G., 1995. Phosphatic nodules in the outer continental shelf off Madras, Bay of Bengal. *Indian J. Mar. Sci.* 24, 8–12.
- | Vaz, G.G., Faruque, B.M., Biswas, N.R., Vijaykumar, P., Misra, U.S., Sankar, J., Rao, J.V.K., 1996. Phosphorite from the upper continental slope off Kachchh, northwest coast of India. *Indian J. Mar. Sci.* 25, 20–24.
- | Vaz, G.G., Vijaykumar, P., Rao, B.L., 1999. Phosphorite from the Continental Margin off Madras, Bay of Bengal. *Mar. Georesources Geotechnol.* 17, 33–48. doi:10.1080/106411999273990
- | Wright, J., Seymour, R.S., Shaw, H.F., 1984. REE and Nd isotopes in conodont apatite: Variations with geological age and depositional environment, in: Clark, D.L. (Ed.), *Conodont Biofacies and Provincialism*. Geological Society of America, pp. 325–340. doi:10.1130/SPE196-p325
- | Wyrski, K., 1973. *Physical Oceanography of the Indian Ocean*. Springer Berlin Heidelberg, pp. 18–36. doi:10.1007/978-3-642-65468-8\_3

Formatted: Space After: 12 pt

**Table 1:** Sampling details, sedimentation rates, bottom water oxygen concentration, diffusive flux of P and its burial efficiency

Station Name	Latitude (N)	Longitude (E)	Depth (m)	Sedimentation Rate (cm/ky)	Bottom water oxygen concentration ( $\mu\text{mol/L}$ )	Diffusive flux of P ( $\text{mmol m}^{-2} \text{yr}^{-1}$ )	Burial Efficiency (PBE) (%)
SPC 1R	14°46.10'	72°40.35'	347	3.8	6.29	-16	2.1
SPC 2	14°16.25'	72°52.45'	325	2.1	7.49	-22	2.6
SPC 4R	12°55.10'	73°33.46'	279	26.5	9.32	-1.1	90

**Table 2:** The equations used for integration of area under the curve for cores SPC-1R and SPC-2. Also tabulated are depth integrated  $P_{auth}$  content increase versus depth integrated  $P_{org}$  and  $P_{bio}$  decrease using these equations

1. The equations for the curves integrated for SPC 1R:

$$P_{org} \ y = -13.59\ln(x) - 34.675 \quad R^2 = 0.93$$

$$P_{bio} \ y = -29.02\ln(x) - 67.707 \quad R^2 = 0.59$$

$$P_{auth} \ y = 9.2889\ln(x) + 47.023 \quad R^2 = 0.84$$

2. The equations for the curves integrated for SPC 2:

$$P_{org} \ y = -11.76\ln(x) - 32.269 \quad R^2 = 0.94$$

$$P_{bio} \ y = -17.91\ln(x) - 32.923 \quad R^2 = 0.74$$

$$P_{auth} \ y = 10.19\ln(x) + 43.103 \quad R^2 = 0.65$$

3. The integrated areas under the curves have been converted from units of (g P/g x cm) to units of (gP/cm<sup>2</sup>) using the following equation:

$gP/cm^2 = (1 - \phi)\rho \ (g/cm^3) \text{Area} \ (gP/g \ x \ cm)$  where  $\phi = 0.65$  and  $\rho = 2.65 \ g/cm^3$  (Ruttenberg and Berner, 1993).

Station	Depth interval of integration	Integrated $P_{org}$ deficit (gP/cm <sup>2</sup> )	Integrated $P_{bio}$ deficit (gP/cm <sup>2</sup> )	Integrated $P_{auth}$ increase (gP/cm <sup>2</sup> )
SPC 1R	0-28	0.82±0.01	1.54±0.02	0.99±0.02
SPC 2	0-23	0.51±0.005	1.68±0.005	1.09±0.01



**Figure captions:**

**Figure 1:** Map showing the reported areas of phosphogenesis and phosphorite occurrences along with the areas of high  $P_{\text{auth}}$  content.

**Figure 2:** a) The core locations are plotted on a swath bathymetric depth contour map (contour interval 200 m) showing the mid-slope/marginal highs along with the geophysical transects (modified from Rao et al., 2010); b and c) single channel seismic reflection images of profiles A-A', B-B'; d) multi-channel seismic image of profile F-F' on the southern edge of topographic high (Rao et al., 2010 and references therein)

**Figure 3:** Dissolved phosphate ( $\mu\text{mol/L}$ ) in seawater (with depth) and porewater (with sediment depth). Note the two scales used for the porewater profiles of phosphate.

**Figure 4:** Down core variation of total phosphorus and P in five geochemically separable phases (units in  $\mu\text{mol/g}$ )

**Figure 5:** Relative percentages of solid P phases with sediment depth

**Figure 6:** Downcore variation of total Fe content (wt.% on a carbonate-free basis) in the sediment cores

**Figure 7:** Downcore variation of total organic and inorganic carbon (TOC and TIC in wt%) in a) SPC 1R, b) SPC 2 and c) SPC 4R

**Figure 8:** Downcore variation of a) molar  $C_{\text{org}}/P_{\text{reactive}}$  and b) molar  $C_{\text{org}}/P_{\text{org}}$  ratios

**Figure 9: a)** Downcore variation of molar  $\text{Fe}_{\text{ex}}/P_{\text{Fe}}$  ratios and U/Th ratio in sediments.  $\text{Fe}_{\text{ex}}$  represents the empirically calculated excess Fe concentrations over that found in lithogenic fraction. Also shown are porewater nitrate ( $\mu\text{mol/L}$ ) in SPC1R and SPC2. b) Dissolved oxygen concentration in the water column.

**Figure 10:** Downcore variation of elements Ti, Th, Zr and Rb (in carbonate-free basis) in the three cores showing a large fluctuation in SPC 4R

**Figure 11:** Solid-phase profiles of  $P_{\text{auth}}$ ,  $P_{\text{org}}$  and  $P_{\text{bio}}$  (all in wt. %) and their best fit curves.

**Figure 12:** Downcore profiles of  $P_{\text{react}}$  (Sum of,  $P_{\text{bio}}$ ,  $P_{\text{Fe}}$  and  $P_{\text{org}}$ ) and  $P_{\text{auth}}$  in SPC 4R (unit in  $\mu\text{mol/g}$ )

**Figure 13:** Downcore variation of  $\text{CaCO}_3$ ,  $C_{\text{org}}/N$  ratio and texture of SPC 1R, 2 and 4R



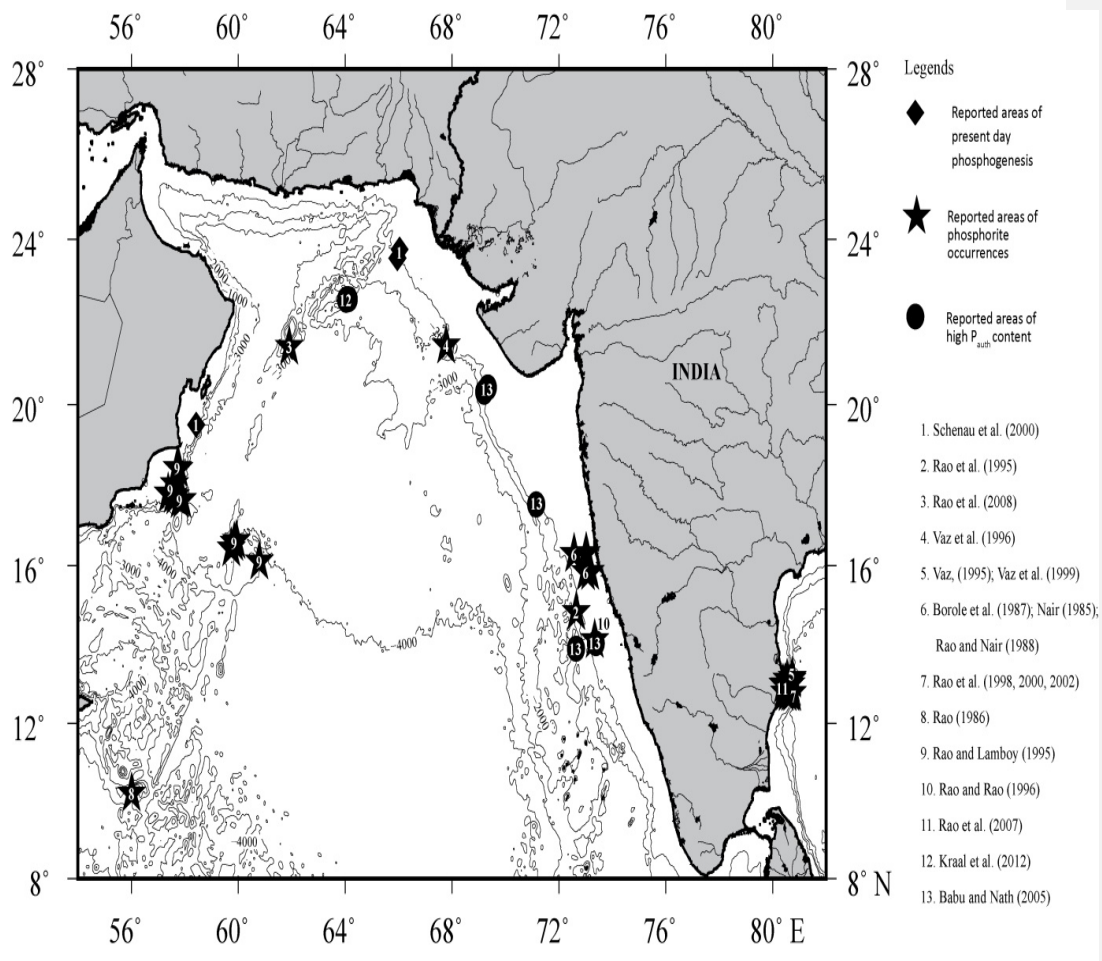


Figure 1

|

|

|

Figure 1

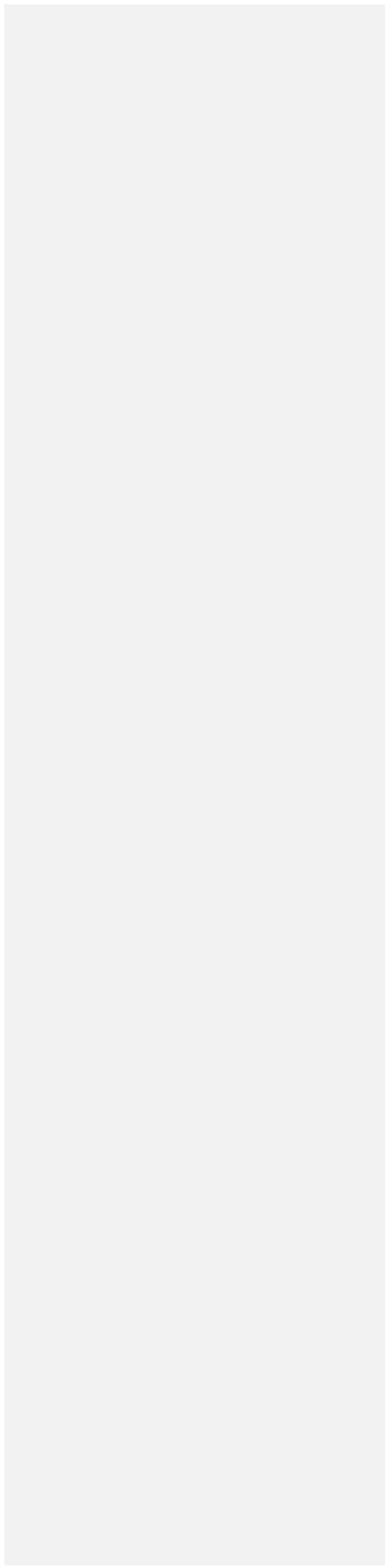
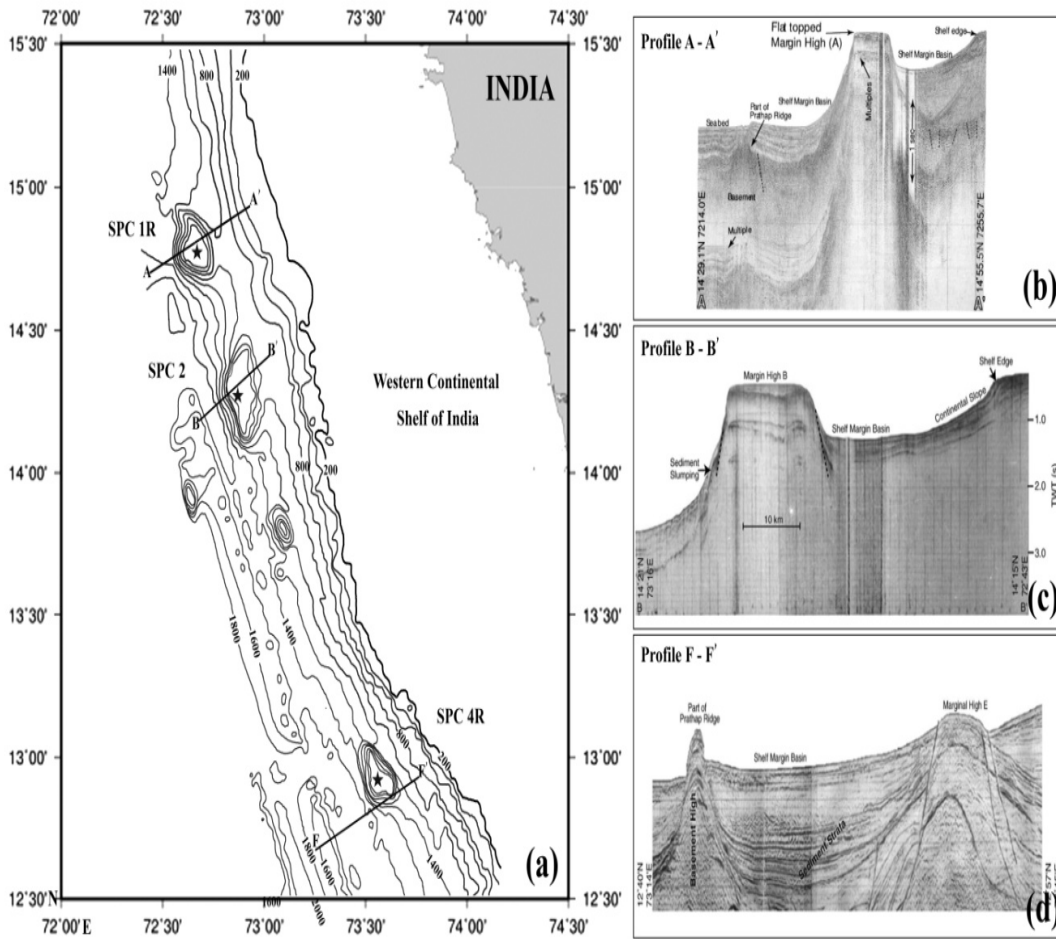


Figure 2



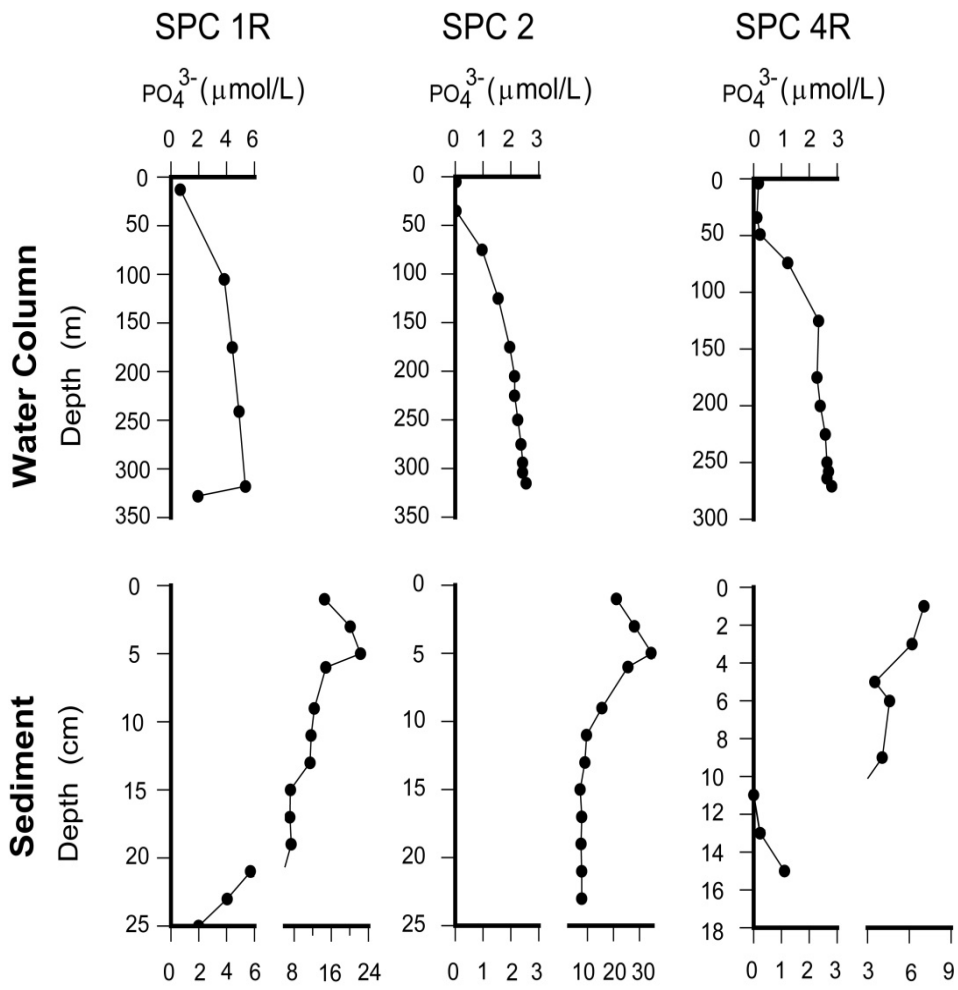


Figure 3

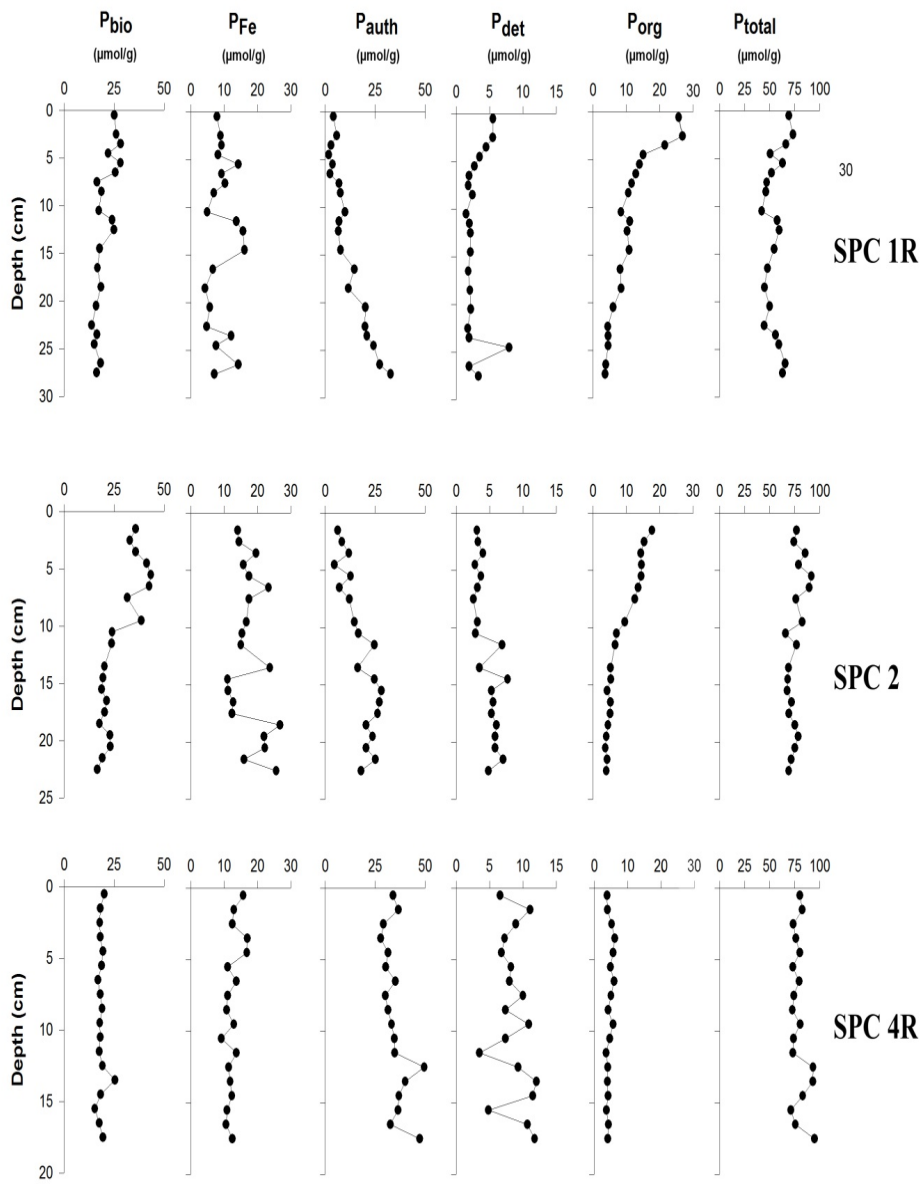


Figure 4

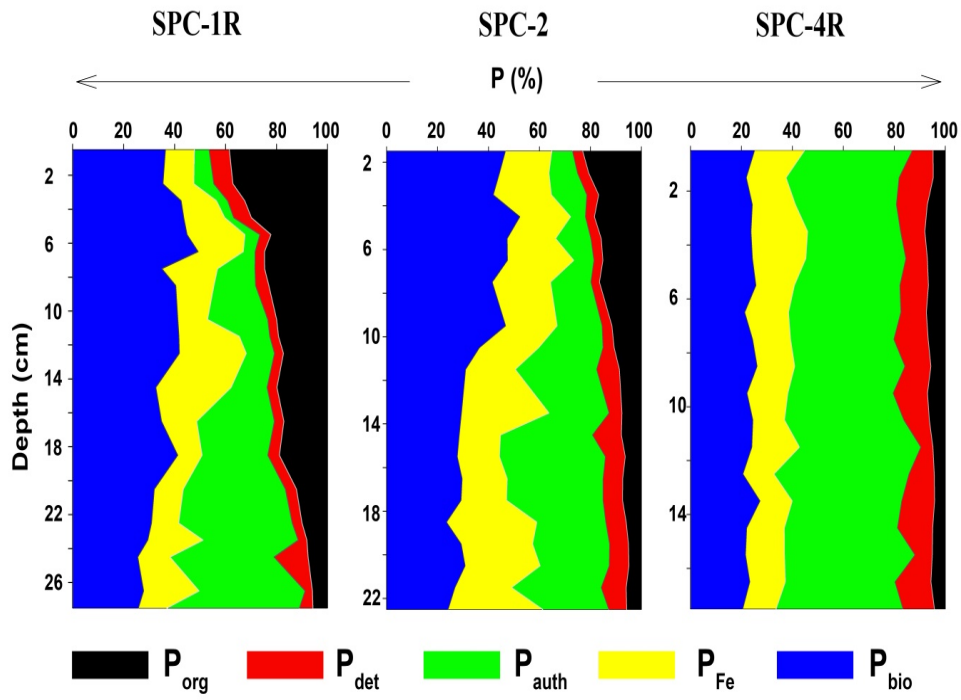


Figure 5



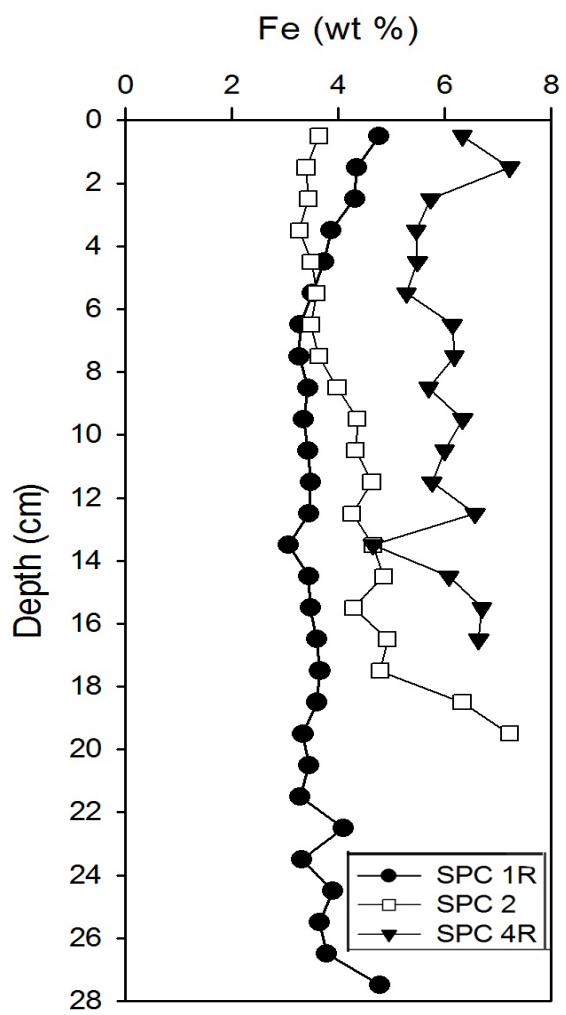


Figure 6

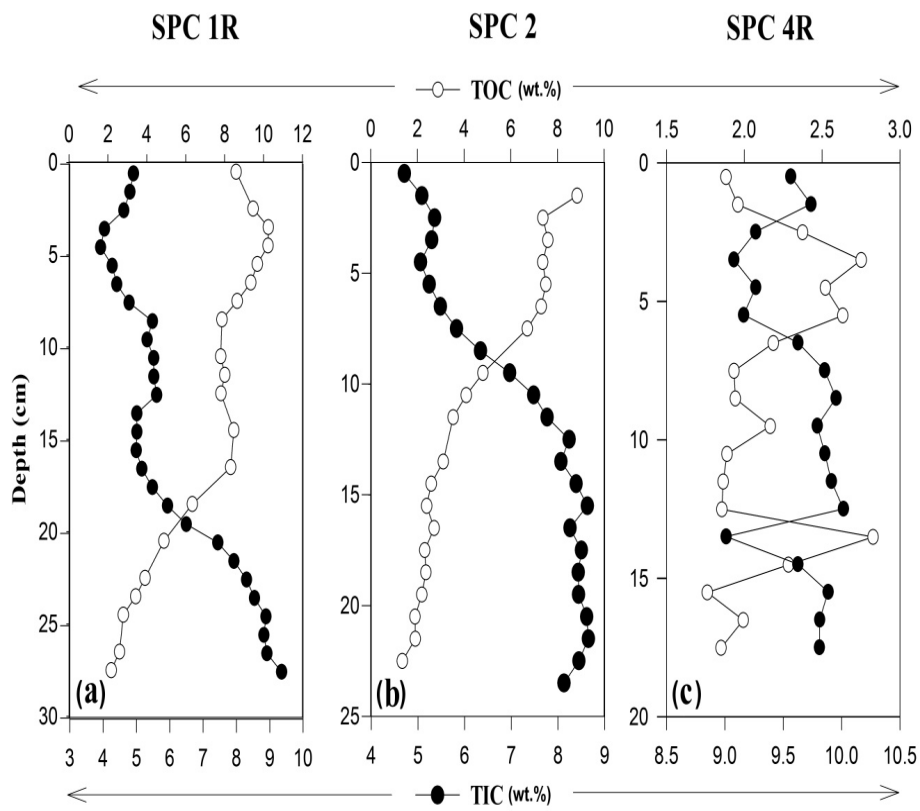


Figure 7

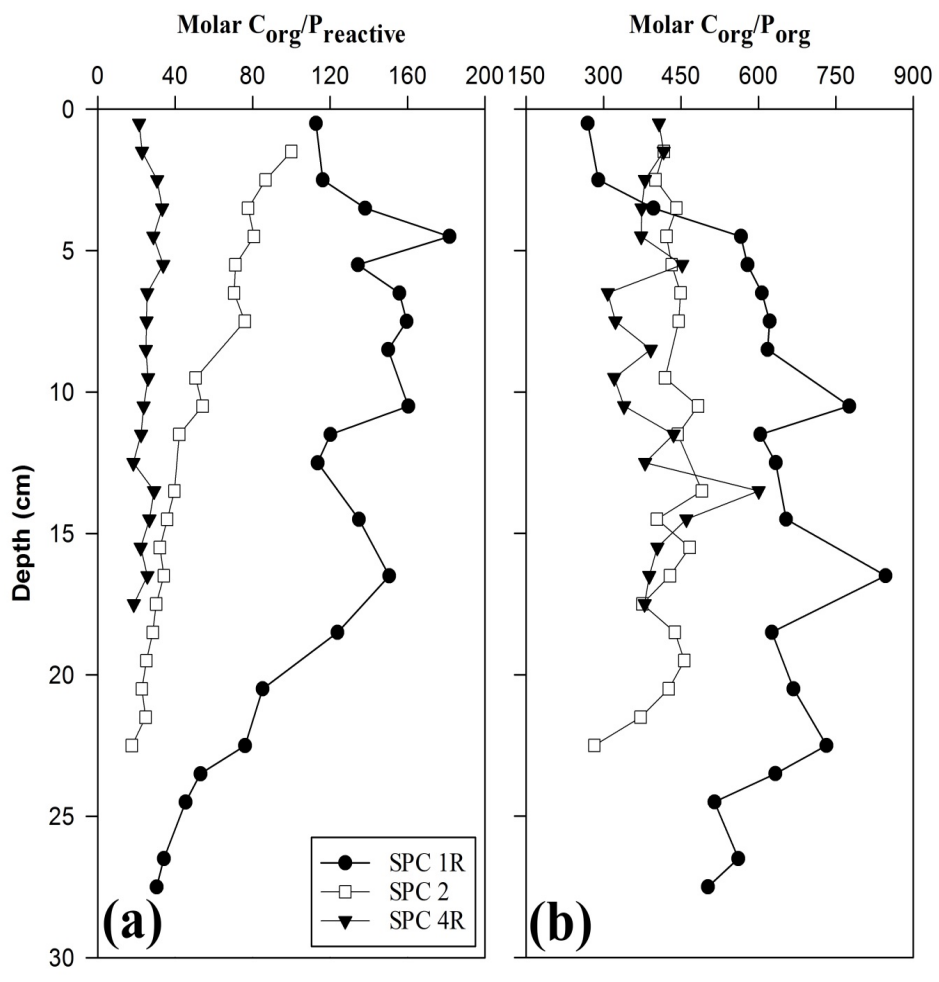


Figure 8

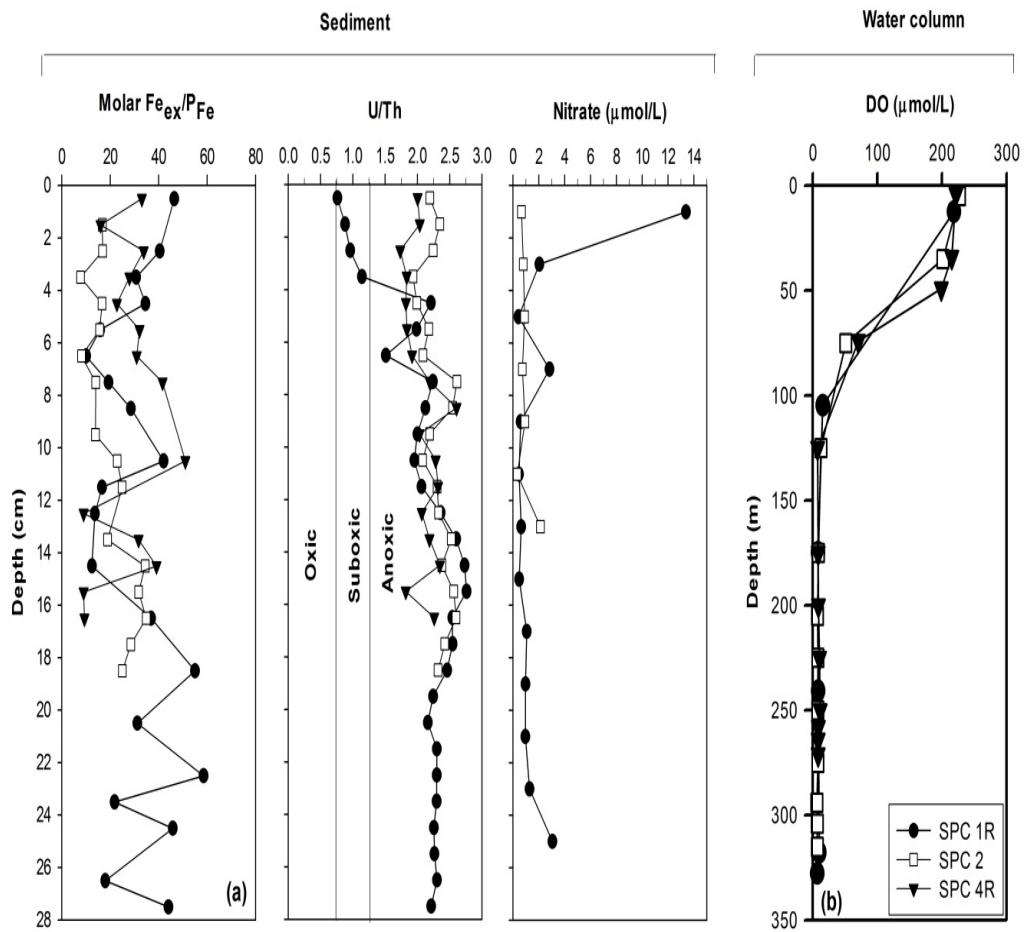
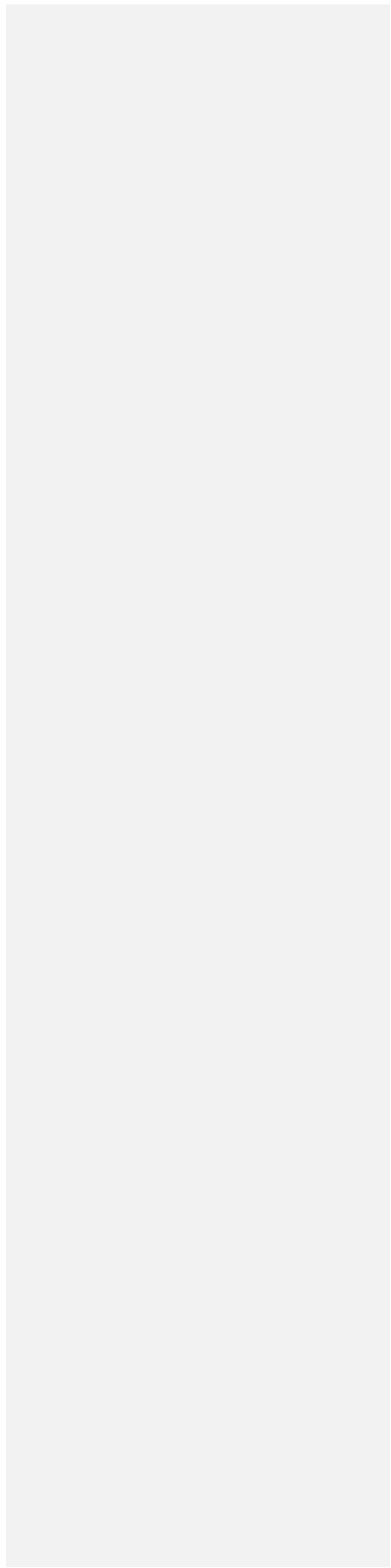


Figure 9

|

|



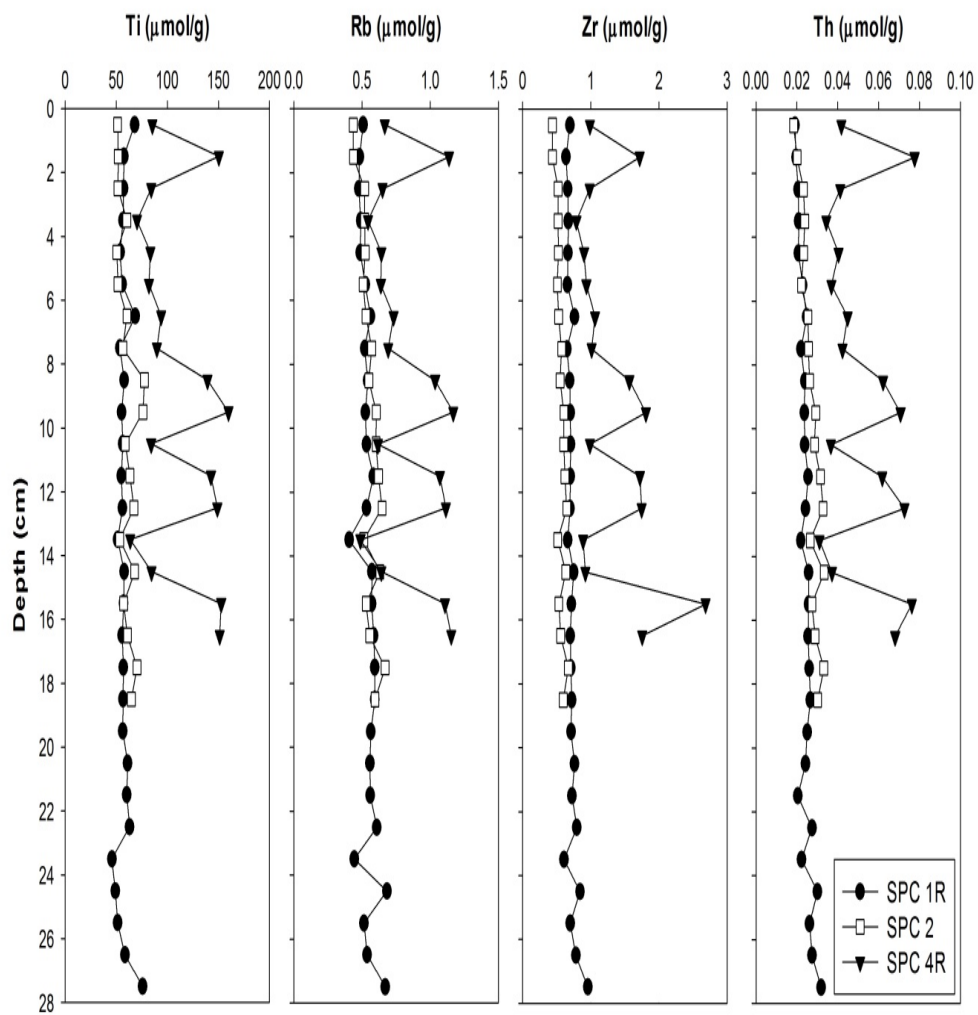
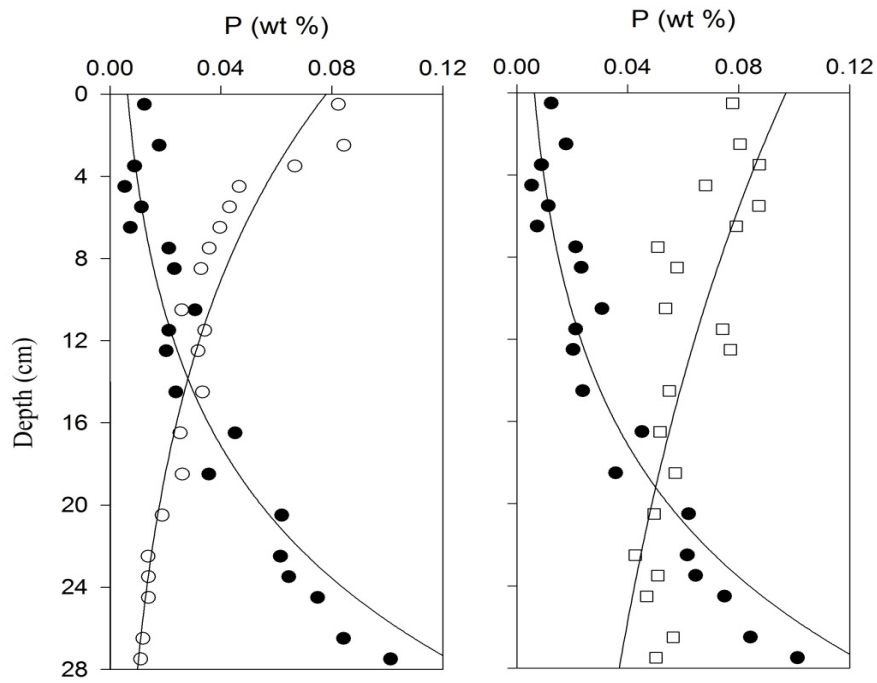


Figure 10

**SPC 1R**



**SPC 2**

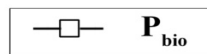
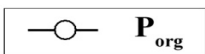
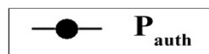
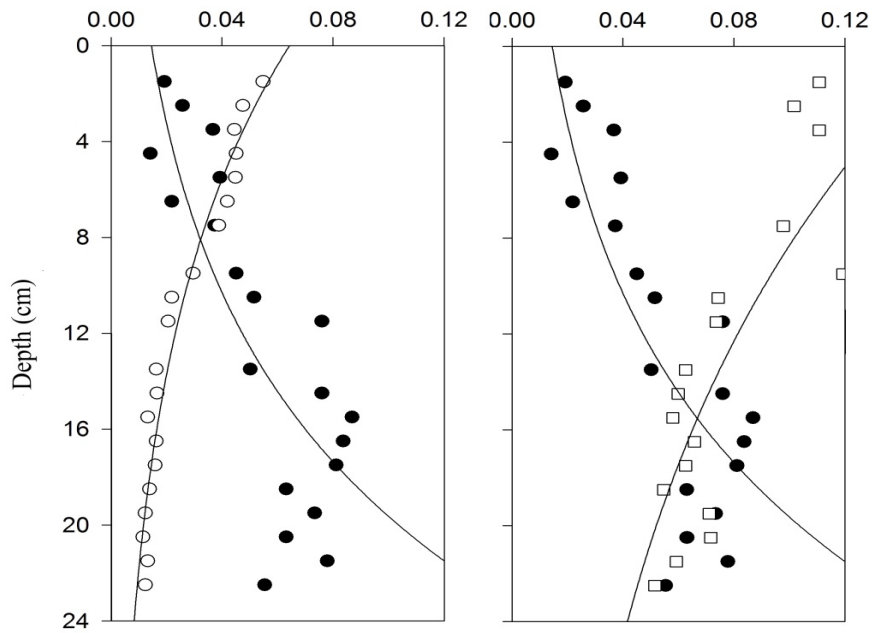


Figure 11

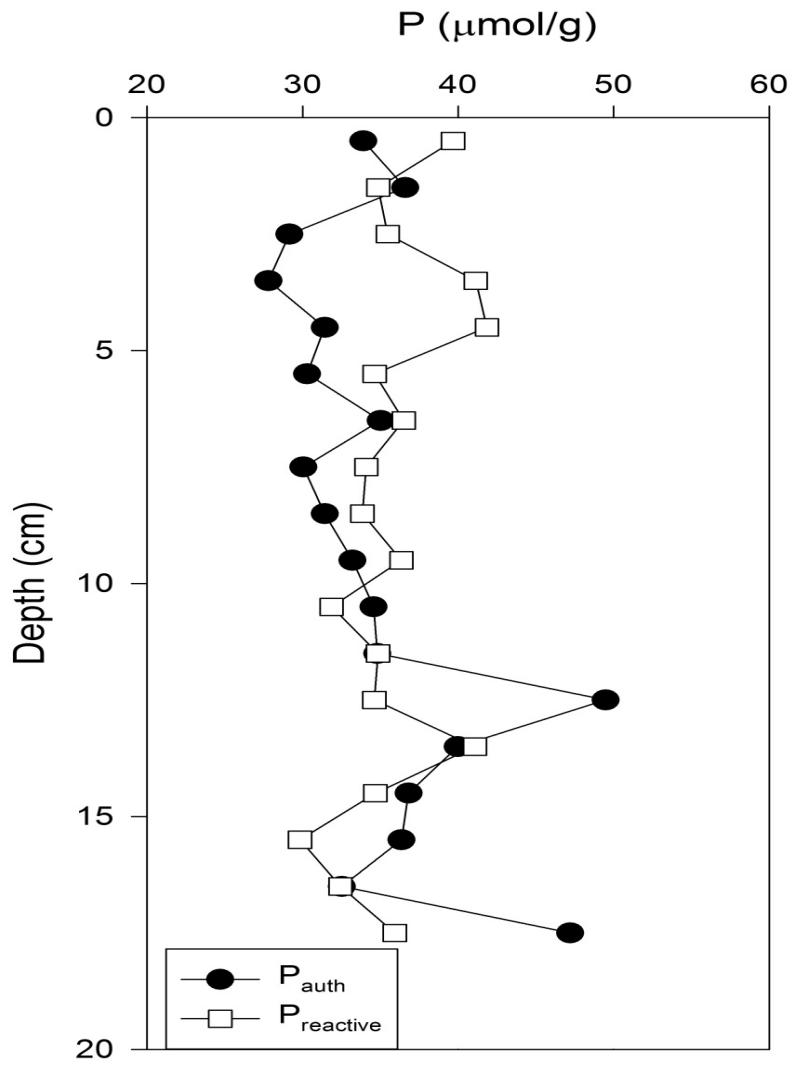


Figure 12



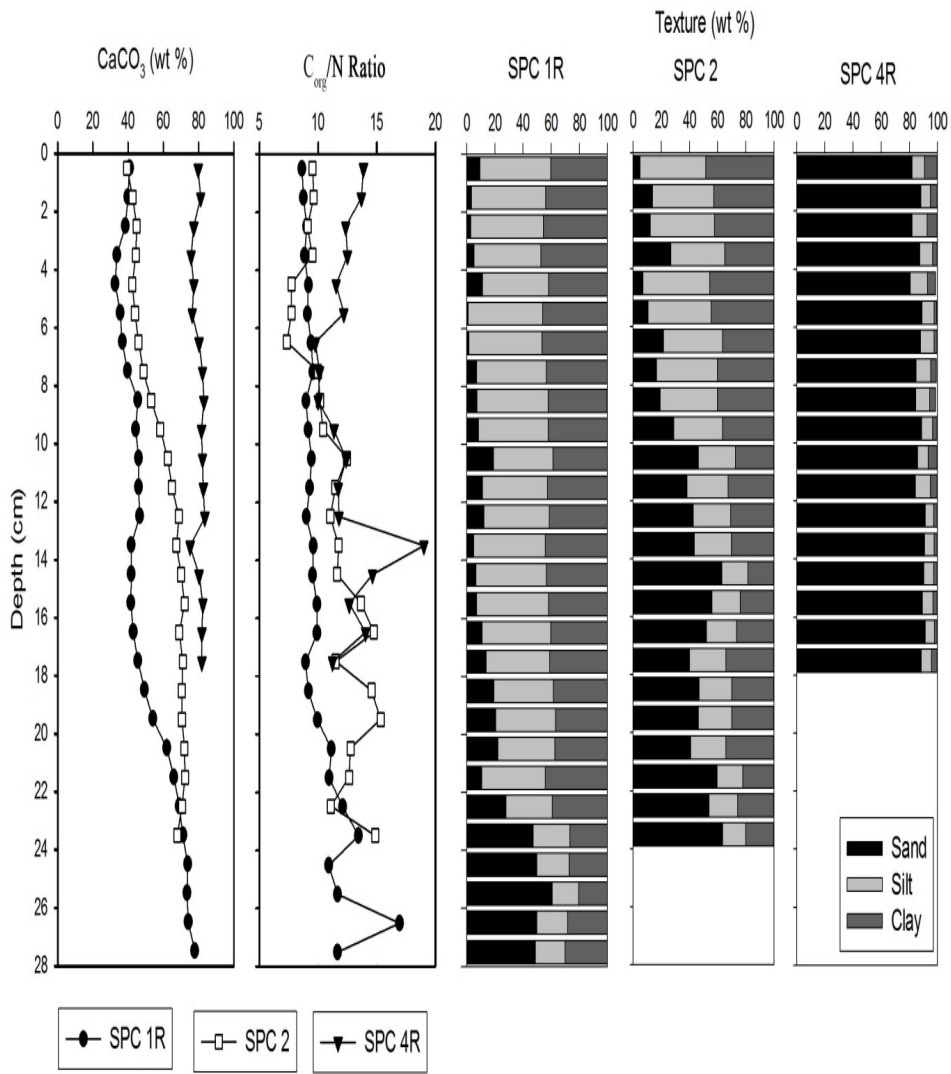


Figure 13